

AD-A123 065

THE MORPHOLOGY OF A MULTI-BUBBLE SYSTEM IN THE  
IONOSPHERE(U) NAVAL RESEARCH LAB WASHINGTON DC

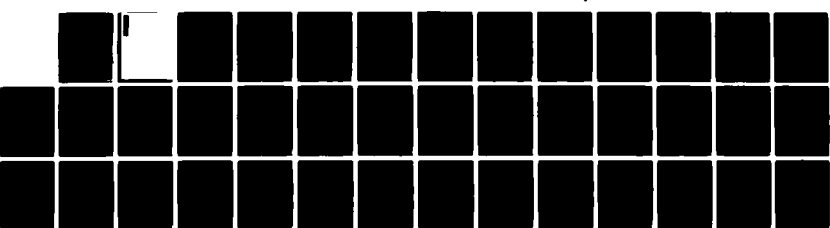
J CHEN ET AL. 11 JAN 83 NRL-MR-5007

1/1

UNCLASSIFIED

F/G 4/1

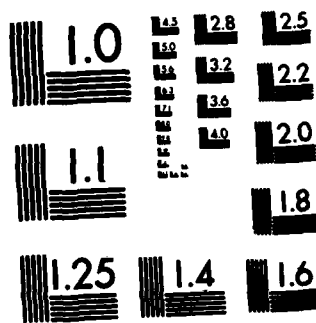
NL



END

DATE  
FILED  
2 83

DTIC



MICROCOPY RESOLUTION TEST CHART  
NATIONAL BUREAU OF STANDARDS-1963-A

AD A123065

SECURITY CLASSIFICATION OF THIS PAGE (When Data Entered)

REPORT DOCUMENTATION PAGE		READ INSTRUCTIONS BEFORE COMPLETING FORM
1. REPORT NUMBER	2. GOVT ACCESSION NO.	3. RECIPIENT'S CATALOG NUMBER
NRL Memorandum Report 5007	AD-A123065	
4. TITLE (and Subtitle) <b>THE MORPHOLOGY OF A MULTI-BUBBLE SYSTEM IN THE IONOSPHERE</b>		5. TYPE OF REPORT & PERIOD COVERED Interim report on a continuing NRL problem.
7. AUTHOR(s) J. Chen*, P. Satyanarayana*, and S.L. Ossakow		6. PERFORMING ORG. REPORT NUMBER
9. PERFORMING ORGANIZATION NAME AND ADDRESS Naval Research Laboratory Washington, DC 20375		10. PROGRAM ELEMENT, PROJECT, TASK AREA & WORK UNIT NUMBERS 61153N; RR033-02-44; 47-0883-0-3; 47-0889-0-3
11. CONTROLLING OFFICE NAME AND ADDRESS Office of Naval Research      Defense Nuclear Agency Arlington, VA 22217      Washington, DC 20305		12. REPORT DATE January 11, 1983
14. MONITORING AGENCY NAME & ADDRESS (if different from Controlling Office)		13. NUMBER OF PAGES 39
		15. SECURITY CLASS. (of this report) <b>UNCLASSIFIED</b>
		15a. DECLASSIFICATION/DOWNGRADING SCHEDULE
16. DISTRIBUTION STATEMENT (of this Report)  Approved for public release; distribution unlimited.		
17. DISTRIBUTION STATEMENT (of the abstract entered in Block 20, if different from Report)		
18. SUPPLEMENTARY NOTES *Present address: Science Applications, Inc., McLean, VA 22102 This research was partially sponsored by the Defense Nuclear Agency under Subtask S99QMXBC, work unit 00067, work unit title "Plasma Structure Evolution," and partially by the Office of Naval Research.		
19. KEY WORDS (Continue on reverse side if necessary and identify by block number)  Equatorial Spread F      Rise velocity Multi-bubble system      Striation fingers Analytic model		
20. ABSTRACT (Continue on reverse side if necessary and identify by block number)  → A multi-bubble model is developed to study the morphology of a finite array of plasma density depletions (bubbles) in the context of equatorial F-region irregularities during spread F. The Pedersen current conservation equation with quasi-neutrality is solved analytically using an electrostatic analogy. The solution is exact with no <i>a priori</i> assumption regarding the separation distance. A two-bubble system with a piecewise constant density profile is first analyzed and the technique is then applied to multi-bubble systems to calculate the polarization electric field and the rise velocities. It is shown that the →		

(Continues)

DD FORM 1 JAN 73 1473

EDITION OF 1 NOV 68 IS OBSOLETE  
S/N 0102-014-6601

SECURITY CLASSIFICATION OF THIS PAGE (When Data Entered)

20. ABSTRACT (Continued)

influence of the neighboring bubbles is relatively short-ranged and that a small number of bubbles can adequately model the essential physics in a large array of bubbles. For moderately short separation distances, it is found that the  $E \times B$  rise velocity is substantially reduced in comparison with the single-bubble case and that the rise velocity is strongly sheared resulting in the deformation of the contours. The implications of the new morphological results on the stability and dynamical behavior of the bubbles are discussed. The analysis can also be applied to a multi-plasma density enhancement (striation fingers and plasma clouds) system such as one might encounter in plasma cloud striation fingers. ←

## CONTENTS

I. INTRODUCTION .....	1
II. A TWO-BUBBLE MODEL .....	3
A. Formulation .....	3
B. The Method of Image Dipoles .....	6
C. Applications .....	10
III. A MULTI-BUBBLE MODEL .....	13
IV. SUMMARY AND DISCUSSION .....	22
ACKNOWLEDGEMENTS .....	23
REFERENCES .....	24



Accession For	
NTIS GRA&I	<input checked="" type="checkbox"/>
DTIC TAB	<input type="checkbox"/>
Unannounced	<input type="checkbox"/>
Justification	<input type="checkbox"/>
By _____	
Distribution/ _____	
Availability Codes _____	
Avail and/or	Special
At	
A	

## THE MORPHOLOGY OF A MULTI-BUBBLE SYSTEM IN THE IONOSPHERE

### I. INTRODUCTION

The behavior of ionospheric plasma has been extensively studied with the aim of understanding various ionospheric phenomena including equatorial spread F (ESF) and plasma cloud striations (see the following reviews: Ossakow, 1979; Fejer and Kelley, 1980; Ossakow, 1981; Kelley and McClure, 1981; Ossakow et al., 1982). In particular, ESF is thought to be initiated by the Rayleigh-Taylor instability, first proposed by Dungey (1956). In the context of this idea, the plasma density depletions resulting from the instability acquire upward polarization induced  $E \times B$  drift velocities. A large body of literature has since been developed to describe the linear and nonlinear properties of Rayleigh-Taylor plasma density irregularities under various assumptions [Haerendel, 1975; Balsley et al., 1972; Chaturvedi and Kaw, 1975a,b; Hudson and Kennel, 1975]. In particular, considerable attention has been given to the morphology and motion [Scannapieco and Ossakow, 1976; Ossakow and Chaturvedi, 1978; Ott, 1978; Hudson, 1978; Anderson and Haerendel, 1979; Ossakow et al., 1979; Zalesak and Ossakow, 1980; Zalesak et al., 1982] of plasma depletions ("bubbles") in the equatorial ionosphere. Moreover, a number of observations [Woodman and LaHoz, 1976; Kelley et al., 1976; Hanson and Sanatani, 1971; McClure et al., 1977; Szuszczewicz et al., 1980, 1981] have indicated the presence of rising plasma bubbles.

Another phenomenon of interest is that of the striations in (artificial) plasma "clouds" (density enhancements). This effect has been attributed to the  $E \times B$  gradient drift instability [Linson and Workman, 1970; Volk and Haerendel, 1971] and appears to be amenable to treatments similar to ESF [Scannapieco and Ossakow, 1976; Scannapieco et al., 1976; Ossakow and Chaturvedi, 1978]. The Rayleigh-Taylor instability and the  $E \times B$  gradient drift instability are both interchange modes that may occur in the leading edge of plasma bubbles and backside of clouds respectively. In both cases, the resulting density depletions and enhancements are thought to drift by the polarization induced  $E \times B$  drift. The electric field is produced by the polarization of the plasma across the earth's magnetic field. The essential ingredient is the small but nonzero ion-neutral collision frequency.

As a result of the initial instability such as the Rayleigh-Taylor instability, an array of density depletions are formed with the wave vector perpendicular to the earth's magnetic field. Moreover, the leading edge of a bubble itself is Rayleigh-Taylor unstable resulting in further "bifurcation" [Ossakow and Chaturvedi, 1978]. Similarly, the  $E \times B$  instability causes the backside of an initial cloud to striate, forming "finger-like" structures. Thus, the plasma depletions and enhancements typically occur in multitudes. Indeed, McClure et al., (1977) and Szuszczewicz et al., (1980;1981) have given evidence for multiple bubbles. In the previous theoretical and numerical simulation works [Ossakow and Chaturvedi, 1978; Anderson and Haerendel, 1979; Zalesak and Ossakow, 1980; Overman et al., 1982], the morphology and evolution have been studied using one-bubble models or a uniformly distributed array of bubbles (clouds). As a result, the intrinsic influence of neighboring bubbles on each other has not been well quantified. Because the bubbles rise due to the polarization induced  $E \times B$  drift, the electric field configuration in and around the bubbles is of central importance.

In the present paper, we study the structure of electrically interacting multi-bubble systems and seek to identify the nature and effects of the mutual interaction. For this purpose, we start with a simple two-bubble configuration in the context of a fluid description and with the emphasis on identifying the basic physics. A simple piecewise-constant density profile is used and the electric field inside and outside the bubbles is obtained analytically by the method of images. The method is then applied to multi-bubble configurations. In a sense, the present work is a non-trivial extension of the single bubble work of Ossakow and Chaturvedi (1978).

The scope of the present paper is limited to discussing the morphology of multi-bubble systems and the time-dependent evolution is not explicitly considered. However, the implications of the results will be discussed in the context of the behavior of bubbles consistent with the approximations used in the analysis. Although we primarily discuss the ESF plasma density depletions (bubbles), the technique developed here can be extended straightforwardly to the treatment of plasma density enhancements (clouds).

In Section II, we develop a two-bubble model based on an electrostatic (dielectric) analogy and solve the current conservation equation with quasi-neutrality for the electric field. Section III describes a multi-bubble model and section IV contains the discussion.

## II. A TWO-BUBBLE MODEL

### A. Formulation

In the present paper, we consider the electric field configuration of electrically interacting multi-bubble systems imbedded in a uniform background plasma and neutral gas. In order to illustrate the basic physics and the theoretical method, we first develop a simple two-bubble model. For his purpose, we adopt a sharp-boundary density profile in which the plasma density is piecewise constant, being uniform inside ( $n_1$ ) and outside ( $n_2$ ) the bubbles and having a discontinuity at the bubble boundaries [Haerendel, 1973; Ossakow and Chaturvedi, 1978; Overman et al., 1982]. The bubbles are modelled by two-dimensional cylinders at the same altitude with circular cross-sections and the axis of the cylinders are aligned with the earth's magnetic field which is assumed to be uniform along the positive z-axis. No neutral wind is included. Figure 1 shows schematically the geometry and the coordinate system. The bubbles are located at  $x = -x_0$  and  $x = x_0$  so that the inter-bubble separation distance is  $2x_0$ . For reference purposes, we denote the cylinders by C1 and C2, respectively. The radius of each bubble is  $a$ . In the equatorial and low latitude regions, the x-axis is along the east-west direction and the gravitational force is along the negative y-axis.

The basic equations in our model are the particle conservation, momentum conservation and current conservation equations [see, for example, Ossakow, 1981]. In addition, quasi-neutrality can generally be assumed on the time scales of interest. In the present paper, we study the morphology of two- and multi-bubble systems by solving the current conservation equation to obtain the instantaneous electric field perpendicular to the magnetic field.

The current conservation equation with quasi-neutrality is

$$\nabla \cdot \underline{J} = 0 \quad (1)$$

where  $\underline{J}$  is the plasma current density due to ion and electron drifts. Neglecting the inertia terms in the momentum equations for cold ion and electron fluids, the current density in the lab frame can be expressed as (see, for example, Ossakow et al., 1979)

$$\underline{J} = en \left[ \frac{1}{\Omega_i} \underline{g} \times \hat{\underline{z}} + \frac{v_{in}}{\Omega_i} \left( \frac{1}{\Omega_i} \underline{g} + \frac{c}{B} \underline{E} \right) \right], \quad (2)$$

where  $\Omega_i = eB/m_i c$  is the ion cyclotron frequency,  $\hat{\underline{z}}$  is the unit vector along the earth's magnetic field,  $\underline{g}$  is the gravitational acceleration,  $n$  is the plasma density, and  $v_{in}$  is the ion-neutral collision frequency. In (2), we have used the fact that  $m_e/m_i \ll 1$  and have neglected the electron  $\underline{g} \times \hat{\underline{z}}$  contribution. In addition, in arriving at (2), we have made the approximation  $v_{in}/\Omega_i \ll 1$ . In the F region,  $v_{in}/\Omega_i$  is typically of the order of  $10^{-2}$  or less.

The second term in the square brackets in (2) gives the force-field ( $\underline{g}$  and  $\underline{E}$ ) aligned drift currents due to the finite ion-neutral collisions. It is convenient to separate the electric field  $\underline{E}$  according to

$$\underline{E} = \tilde{\underline{E}} - \frac{m_i}{e} \underline{g}.$$

The term  $(-m_i/e) \underline{g}$  is the component of  $\underline{E}$  cancelling the drift along the gravitational field so that the net drift perpendicular to the magnetic field is described by  $\tilde{\underline{E}}$ . Then, the current  $\underline{J}$  can be written as

$$\underline{J} = \sigma \underline{E}_J \quad (3)$$

where

$$\sigma \equiv v_{in} \frac{nec}{B\Omega_i}$$

and

$$\underline{E}_J \equiv \tilde{\underline{E}} + \frac{B}{cv_{in}} \underline{g} \times \hat{\underline{z}}. \quad (4)$$

Here,  $\underline{B}$  and  $\underline{g} = -gy$  are assumed to be uniform. Physically,  $\underline{E}_J$  can be thought of as the electric field driving the current  $\underline{J}$  perpendicular to the magnetic field in the frame moving with the velocity  $\underline{v}_d = -\omega_i^{-1} \underline{g} \times \underline{z}$  relative to the lab frame and  $\sigma$  may be identified as the Pedersen conductivity due to  $v_{in} \neq 0$ .

Equation (1) can now be written in the equivalent form

$$\underline{\nabla} \cdot (\underline{n} \tilde{\underline{E}}) = -\frac{\underline{B}}{cv_{in}} (\underline{g} \times \underline{z}) \cdot \underline{\nabla} n. \quad (5)$$

Perkins et al. (1973) obtained this expression and noted that (5) describes a dielectric immersed in a uniform electric field  $\underline{E}_0$  where

$$\underline{E}_0 = \frac{\underline{B}}{cv_{in}} \underline{g} \times \underline{z}. \quad (6)$$

In an earlier work, Longmire (1970) utilized a similar magnetostatic analogy to treat the motion of isolated ion clouds. Ossakow and Chaturvedi (1978) used (5) to analytically study a single bubble system. In this dielectric analogy,  $\tilde{\underline{E}}$  is the polarization (self) electric field of the bubbles in the uniform field  $\underline{E}_0$  and  $\underline{E}_J$  corresponds to the total electric field  $(\underline{E}_0 + \tilde{\underline{E}})$  satisfying the boundary conditions across the bubble boundaries,

$$\begin{aligned} (\sigma \underline{E}_J)_\perp &= \text{continuous} \\ (\underline{E}_J)_\parallel &= \text{continuous} \end{aligned} \quad (7)$$

and at infinity ( $x, y \rightarrow \infty$ )

$$\underline{E}_J \rightarrow \underline{E}_0. \quad (8)$$

Note that we have implicitly chosen a reference frame in which the electric field of the distant undisturbed ionosphere is  $\underline{E}_0$ . The symbols  $\perp$  and  $\parallel$  refer to the directions parallel and perpendicular to the boundary surfaces, respectively. In the present paper, we also adopt the dielectric analogy and solve the current conservation equation (1) subject to the above boundary conditions (7) and (8). For this purpose, it is illuminating to

rewrite equation (1) as

$$\underline{\nabla} \cdot (\sigma \underline{E}_J) = 0 \quad (9)$$

In the following section, we describe the method of image dipoles used to solve this "dielectric equation". As a matter of notation, in the remainder of the paper, we use  $\underline{E}$  without the subscript  $J$  to denote the solution of (9).

### B. The Method of Image Dipoles

The problem of solving Poisson's equation (9) with multiple disconnected boundaries is generally difficult. However, in the case treated here with circular cross-sections, the dielectric analogy allows us to construct an exact solution. Consider first a single dielectric cylinder of radius  $a$  centered at  $x = 0$  and a line charge density  $q$  located at  $x = b$  ( $|b| > a$ ). It is well known (Smythe, 1968) that the induced electric field outside the cylinder is that of a line charge  $q' = -q(1-K)/(1+K)$  located at  $x = a^2/b$  and a line charge  $-q'$  located at  $x=0$ . The quantity  $K$  is the ratio of the dielectric constant ( $\sigma_1$ ) inside the cylinder to that outside the cylinder ( $\sigma_2$ )

$$K \equiv \frac{\sigma_1}{\sigma_2} . \quad (10)$$

The induced electric field inside the cylinder is that of a single line charge  $q'' = 2q/(1+K)$  located at  $x = b$ . If we replace the line charge  $q$  by a line dipole moment  $\underline{P}_0 = P_0 \underline{x}$  which is equivalent to two equal and opposite line charges separated by a vanishingly small distance, then we find that the electric field due to polarization of the cylinder is that of a single image dipole  $\underline{P}$  given by

$$\underline{P} = - \left( \frac{1-K}{1+K} \right) \frac{a^2}{b^2} \underline{P}_0, \quad (11)$$

located at  $x = a^2/b$ . Note that no image dipole is present on the axis (to be contrasted with the line charge case) and that  $\underline{P}_0$  and  $\underline{P}$  are colinear, pointing in the opposite directions. The induced electric field inside the cylinder is that due to a dipole moment  $\underline{P}^*$  given by

$$\underline{P}^* = \frac{2}{1+K} \underline{P}_0 \quad (12)$$

located at  $x = b$ .

We now consider two identical dielectric cylinders of radius  $a$  centered at  $x = -x_0$  and  $x = x_0$  (see figure 1) immersed in a uniform electric field  $\underline{E}_0$ . Suppose, for the moment, that the two cylinders are non-interacting. Then, for the purpose of calculating the polarization electric field outside the cylinders, each cylinder may be replaced by a dipole moment  $\underline{P}_0$  located at  $x = -x_0$  and  $x = x_0$ , where

$$\underline{P}_0 = \frac{1}{2} \left( \frac{1-K}{1+K} \right) a^2 \underline{E}_0 \hat{x}, \quad (13)$$

and  $K$  is defined by equation (10). The components of the self electric field are

$$\underline{E}_x = 2P_0 [f(x+x_0, y) + f(x-x_0, y)], \quad (14)$$

and

$$\underline{E}_y = 2P_0 [h(x+x_0, y) + h(x-x_0, y)], \quad (15)$$

where

$$f(x, y) \equiv \frac{x^2 - y^2}{(x^2 + y^2)^2}, \quad (16)$$

and

$$h(x, y) \equiv \frac{2xy}{(x^2 + y^2)^2}. \quad (17)$$

Here the  $x$ - and  $y$ -components of the electric field due to a dipole  $P_0$  at  $x = x_0$  is  $2P_0 f(x-x_0, y)$  and  $2P_0 h(x-x_0, y)$ , respectively. The electric field  $\underline{E}^*$  inside the bubbles is

$$\underline{E}^* = \frac{2}{1+K} \underline{E}_0. \quad (18)$$

In the remainder of the paper, asterisks will be used to denote the electric fields inside the bubbles and dipole moments producing the fields.

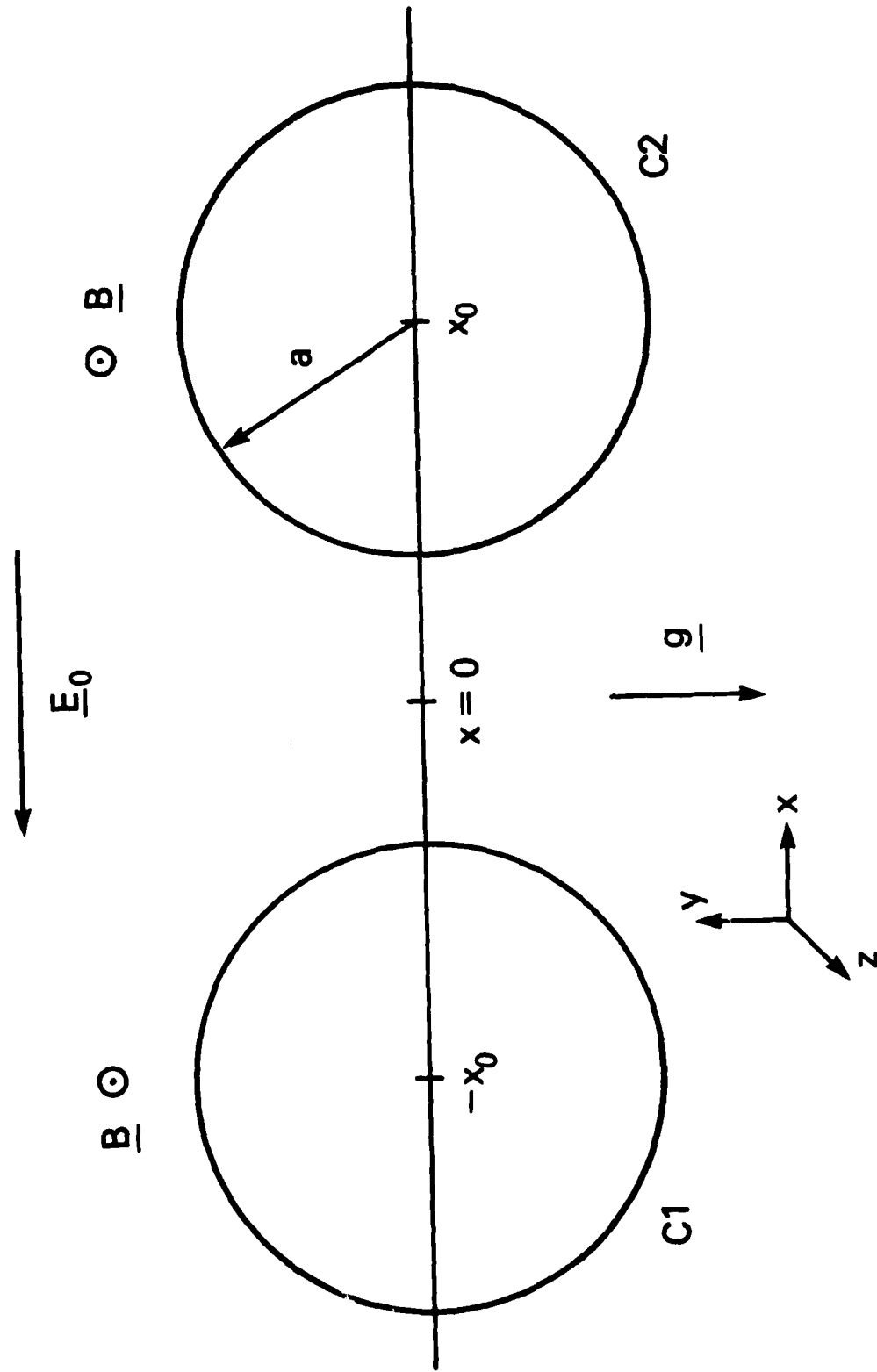


Fig. 1 A schematic drawing of two plasma density depletions and the coordinate system. The depletions have circular cross-sections and are infinite in extent along the  $z$ -direction.

We now allow the two cylinders to interact with each other. In addition to the uniform external field  $E_o$ , each cylinder experiences the dipole field of the other. As a result, each cylinder is further polarized giving rise to image dipoles as given by (11) and (12). Iterating the method of image dipoles described above, it is straightforward to show that the total field outside the bubbles is given by

$$E_x = -E_o + \sum_{n=0}^{\infty} 2P_n [f(x+x_n, y) + f(x-x_n, y)], \quad (19)$$

and

$$E_y = \sum_{n=0}^{\infty} 2P_n [h(x+x_n, y) + h(x-x_n, y)], \quad (20)$$

where  $f$  and  $h$  are defined by (16) and (17). Here, for  $n \neq 0$ ,

$$P_n \equiv -\left(\frac{1-K}{1+K}\right) \frac{a^2}{b_n^2} P_{n-1}, \quad (21)$$

$$b_n \equiv x_o + x_{n-1}, \quad (22)$$

and

$$x_n \equiv x_o - \frac{a^2}{x_o + x_{n-1}}. \quad (23)$$

For  $n = 0$ , we have  $x_n = x_o$  and  $P_0$  is given by (10).

Similarly, the total electric field inside each cylinder, say, (C2) located at  $x = x_o$ , is found to be

$$E_x^* = -\frac{2}{1+K} E_o + \frac{2}{1+K} \sum_{n=0}^{\infty} 2P_n f(x+x_n, y), \quad (24)$$

and

$$E_y^* = \frac{2}{1+K} \sum_{n=0}^{\infty} 2P_n h(x+x_n, y), \quad (25)$$

where  $P_n$  and  $x_n$  are defined above. For the other bubble (C1), the field is obtained by replacing  $x_o$  with  $-x_o$  in the functions  $f$  and  $h$ .

It can be seen from (19)-(23) that the convergence properties of these series depend on the parameter  $s$  defined by

$$s = \frac{1-K}{1+K} \frac{a^2}{(2x_0)^2} . \quad (26)$$

Each successive line dipole moment is reduced by a factor of  $s$  and a geometrical factor of order unity from the preceding one. Since  $x_0 > a$ , we have  $|s| < 1/4$  for any  $K$ . As a result, the series are generally rapidly convergent except for very small center-to-center separation distances ( $x_0 \sim a$ ).

### C. Applications

In order to apply the above dielectric results to the ionospheric bubble and cloud problems in accordance with the dielectric analogy (equations (5) and (6)), we identify the dielectric constant  $\sigma$  with the Pedersen conductivity defined in Section II and recall that  $\underline{E}_0$  is given by equation (6). Note that the Pedersen conductivity is proportional to the plasma density so that

$$K = \frac{n_1}{n_2} ,$$

where  $n_1$  and  $n_2$  are the plasma densities inside and outside the bubbles. With these identifications, equations (19), (20), (24) and (25) describe the electric field of a two-bubble system in the frame moving with  $\underline{v}_d = -\Omega_i^{-1} \underline{g} \times \underline{z}$  relative to the earth. Note that our formalism guarantees that the field components obtained above exactly satisfy equation (9) and the boundary conditions (7) and (8), as can be verified easily. Thus, the solution is unique. It is also worth noting that all the image line dipole moments are aligned with the  $x$ -axis and no higher multipoles such as quadrupole moment arise. If the bubbles are at different heights, the interaction can still be expressed as a series of image dipole moments that are parallel to the  $x$ -axis but the images are not induced on the  $x$ -axis itself.

As a result of the polarization electric field, the plasma bubbles (density depletions)  $\underline{E} \times \underline{B}$  drift. The drift velocity relative to the distant undisturbed ionosphere where the electric field is  $\underline{E}_0$  is given

by  $\underline{V} = c (\underline{E}^* - \underline{E}_0) \times \underline{B}/B^2$ . In particular, the single-bubble rise velocity  $\underline{V}_1$  is (using equation 18)

$$\underline{V}_1 = - \left( \frac{1-K}{1+K} \right) \frac{1}{v_{in}} \underline{g}. \quad (27)$$

For bubbles,  $K < 1$  and  $\underline{V}_1$  is upward. This result has been obtained by Ossakow and Chaturvedi [1978]. Because  $\underline{g}$  is assumed to be uniform, a single isolated bubble maintains its circular cross-section as it rises with the constant velocity  $\underline{V}_1$ . The presence of a second bubble, however, modifies the rise velocity significantly. In particular, it is no longer uniform and the cross-sections do not remain unchanged. We have numerically carried out the summations indicated in (19), (20), (24), and (25). The results are depicted in figure 2. The solid lines represent the self electric field lines or equivalently the Pedersen current lines while the dashed lines correspond to the instantaneous  $\underline{E} \times \underline{B}$  drift velocity ( $\underline{V}_2$ ) for a two-bubble system ( $2x_0 = 2.5a$  and  $K = 0$  for 100% depletion). This figure shows only one quadrant; the actual system is spatially uniform in the  $z$ -direction and is symmetric about the  $y$ - $z$  plane and the  $x$ - $z$  plane. The solid electric field lines are such that the line density is proportional to the field strength. This figure clearly shows that the electric field inside the bubble is significantly modified from the uniform field of an isolated bubble (see (18)). As a general remark, the interaction vanishes as  $K \rightarrow 1$  and the separation distance increases to infinity.

In this example, the electric field strength at the point A ( $x = x_0 - a$ ,  $y = 0$ ) is approximately 1/3 of that at B ( $x = x_0 + a$ ,  $y = 0$ ). The prominently nonuniform electric field inside the bubbles has a number of important implications for the dynamic behavior of the two-bubble system. The drift lines (dashed) in figure 2 show that different regions of a bubble undergo drift in the east-west ( $\underline{x}$ ) direction with respect to the undisturbed ionosphere. This horizontal drift can be a significant fraction of the vertical rise velocity at some points inside the bubble. For example,  $|E_y^*/(E_x^* - E_0^*)| \approx 0.55$  at  $r = a$ , and  $\theta = \pi/8$  where  $r$  is the radial distance from  $x = x_0$ ,  $a$  is just inside the bubble surface and  $\theta$  is measured from the point A ( $\theta = 0$ ). Here,  $x_0 = 1.25$  and  $K = 0$  have been used (figure 2). The reason for the strong divergence in the field lines

## TWO BUBBLES

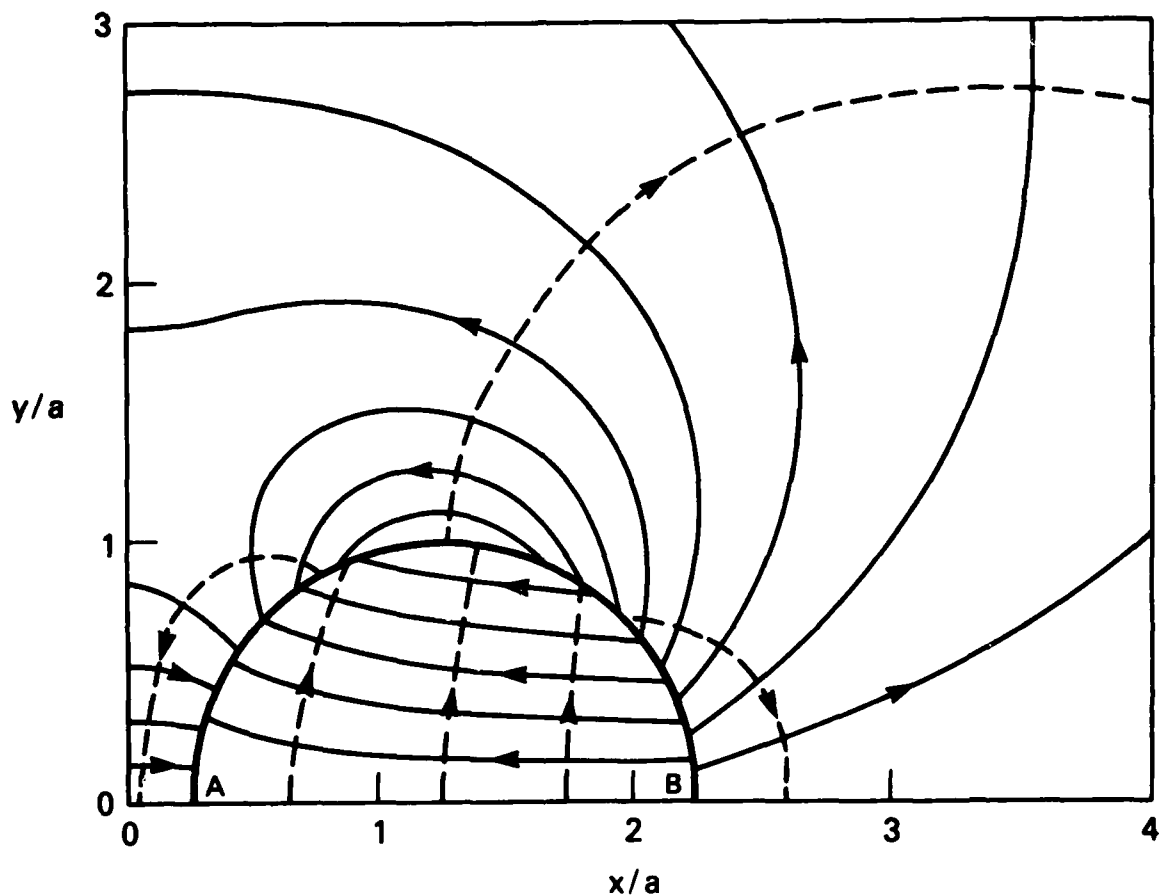


Fig. 2 A drawing of the electric field lines (solid lines) and the  $E \times B$  drift lines (dashed lines) showing one quadrant of a two-bubble system. The system is symmetric about the  $x$ - $z$  plane and  $y$ - $z$  plane. The separation distance is  $2x_0 = 2.5a$  and  $K = 0$  (100% depletion). The points A and B are inside the bubbles at  $x = x_0 - a$  and  $x = x_0 + a$ , respectively.

is that the dipole field due to one bubble opposes the internal field of the other bubble.

Figure 3 shows the two-bubble rise velocity ( $V_y$ ) at a number of points inside the bubble (C2) relative to the uniform rise velocity  $V_1$  of a single bubble given by (27). The ratio  $R_2 \equiv V_y/V_1$  is plotted for the interior points A and B (figure 2) as a function of  $x_0/a$ . We note that the rise velocity  $V_y$  is strongly affected by the neighboring bubble for center-to-center separation distances ( $2x_0$ ) smaller than  $5a$  to  $6a$ . Moreover, comparing  $V_y$  at A and at B, we see that the  $\underline{E} \times \underline{B}$  drift velocity is sheared. This, together with the conclusions of the preceding paragraph, implies that an initially circular cross-section would not remain circular so that the two-bubble system described here does not correspond to a steady-state system. This should be contrasted with single-bubble models in which steady-state solutions are possible for piecewise constant density profiles. Because a neighboring bubble generally introduces nonuniformity in the electric field, it seems difficult to construct a steady-state two-bubble system unless  $x_0/a$  is large.

In interpreting the results, we note that our results do not include the time-dependence. The above field configuration exists if the two-bubble system as described is created at some time (say,  $t = 0$ ). Thus, it would be appropriate as a consistent initial condition for the purpose of studying the subsequent time-evolution. In practice, the drift lines shown in figure 2 are expected to closely approximate the actual evolution for some period of time after  $t = 0$  until the distortion changes the field topology significantly. However, the general feature of the field with the weakest  $x$ -component and hence the slowest rise velocity in the region nearest to the neighboring bubble should remain unchanged in time.

### III. A MULTI-BUBBLE MODEL

In the preceding section, we have discussed in detail a two-bubble model. In considering a multi-bubble system that may be applicable to the ESF phenomenon, the basic physics and the theoretical treatment remain unchanged. However, as the number of bubbles increases, so does the number of image dipoles. For an  $N$ -bubble system, the  $n^{\text{th}}$  order expression must

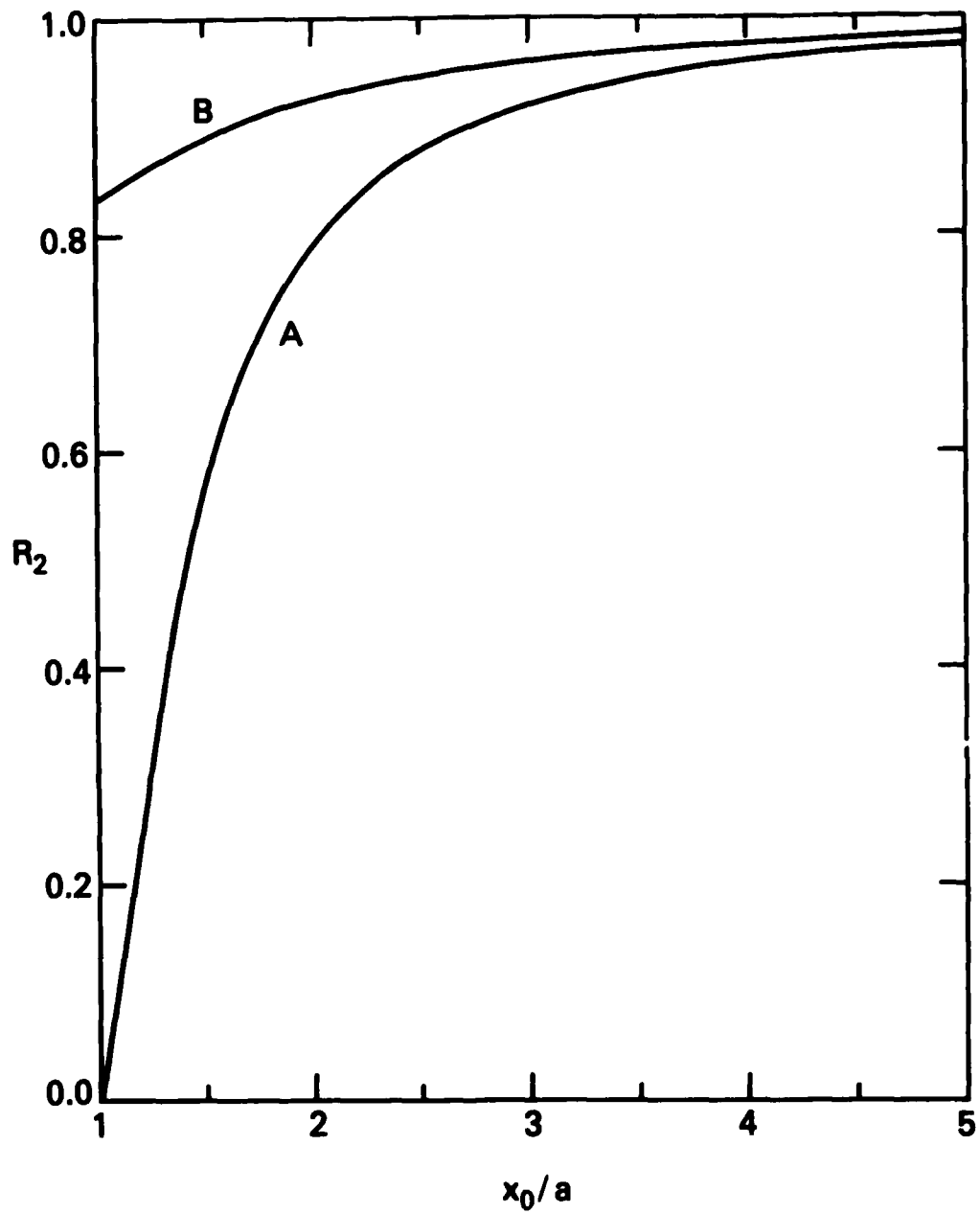


Fig. 3 The ratio  $R_2$  of the vertical rise velocity  $V_2$  of a two-bubble system to the single-bubble rise velocity  $V_1$  (equation (27)) as a function of  $x_0/a$ . The separation distance is  $2x_0 = 2.5a$  and  $K = 0$  (100% depletion). The curve A corresponds to the point A ( $x = x_0 - a$ ) and the curve B to the point B ( $x = x_0 + a$ ) in figure 2.

include  $N(N-1)^n$  image dipoles. Fortunately, the influence of a bubble decreases as the inverse square of the separation distance. Thus, the nearest and the second nearest neighbors are expected to have the dominant effects. A consideration of equations (11) and (12) shows that the second nearest neighbors have effects of the order of  $4^{-2}E_0 \approx 0.06 E_0$  and that the third nearest neighbors have effects of the order of  $6^{-2}E_0 \approx 0.03 E_0$  for a given value of  $a/x_0 < 1$ . This means that the inter-bubble (and also inter-cloud) interaction is short-ranged and that the third nearest neighbors and beyond have no significant influence. Thus, only a small number of bubbles are necessary to model an  $N$ -bubble system with  $N \gg 1$ . Note that the influence of the bubbles still vanishes at infinity, differing from systems satisfying periodic boundary conditions.

The theoretical treatment described is exactly applicable to any  $N$ . However, in the remainder of this section, we include up to a total of 5 mutually interacting bubbles. The mathematical manipulations involved are analogous to those of the preceding section, resulting in series expressions similar to (19), (20), (24), and (25). As before, only dipole moments, not higher multipoles, are induced. Since no new insight is to be gained by examining the actual expressions, we give below only the results. In figure 4, we show the electric field and drift configurations of a system with three plasma depletions. The three depletions are again modelled by cylinders of radius  $a$ , located at  $x = -2x_0, 0$ , and  $2x_0$ . Only one quadrant is shown. The neighboring bubbles are separated by a distance  $2x_0 = 2.5a$ , and are 100% depleted ( $K = 0$ ) as before. The "external" electric field is  $E_0$  given by (6), and the density profile is piecewise constant. The solid lines represent the polarization electric field without  $E_0$ . The quantity  $c(E^* - E_0) \times B / B^2$  is then the instantaneous drift velocity relative to the distant undisturbed ionosphere and is represented by the dashed lines. Although the three-bubble system is different from a two-bubble system in that the former has a central bubble about which the system is symmetric, the general features of the field and drift configurations are similar as can be seen by comparing figures 2 and 4. That is, the field lines and drift lines inside and around the end bubbles of the three-bubble system (figure 4) are similar to those of the two-bubble system (figure 2) because the dominant influence arises from the nearest neighbors. The central bubble in the three-bubble

### THREE BUBBLES

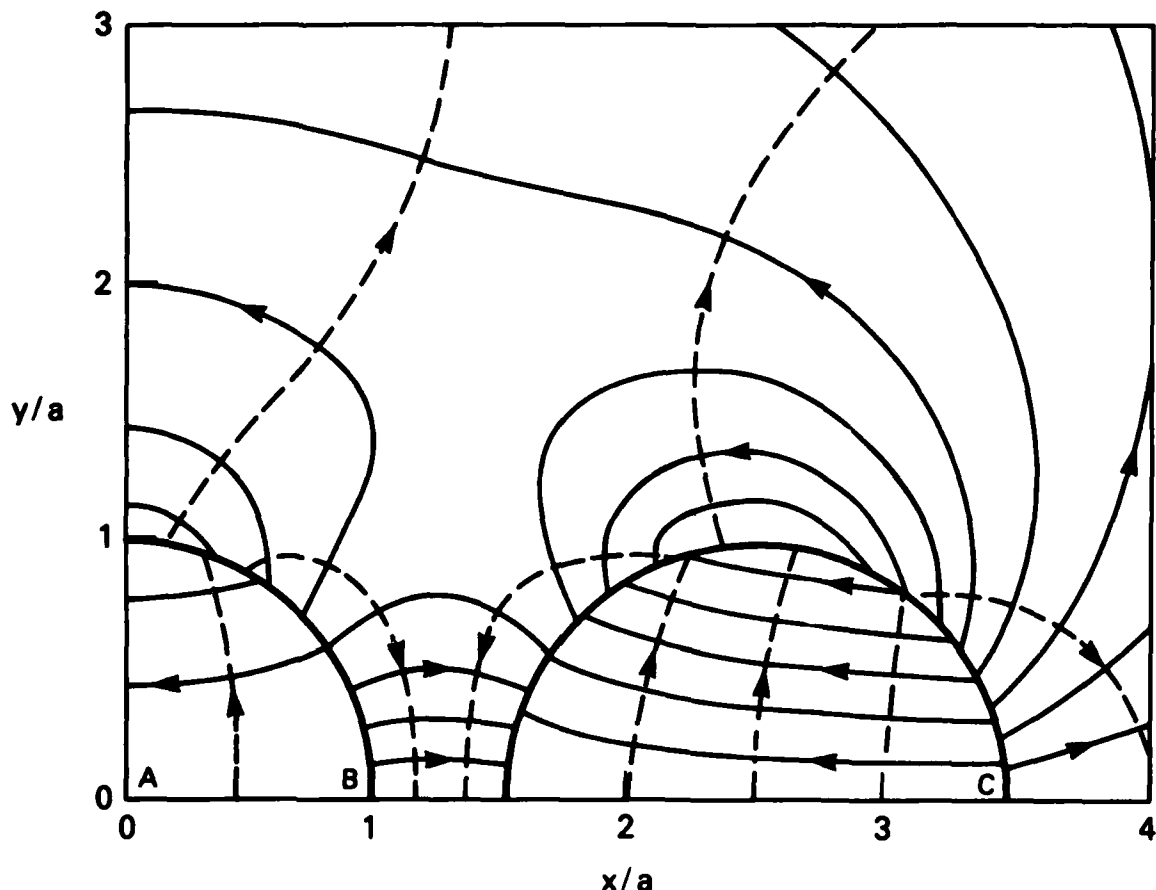


Fig. 4 A drawing of the electric field lines (solid) and the  $\mathbf{E} \times \mathbf{B}$  drift lines (dashed), showing one quadrant of a three-bubble system. The bubbles are placed at  $x = \pm 2x_0$  and  $x = 0$ . The points A, B, and C are inside the bubbles at  $x = 0$ ,  $x = a$ , and  $x = 2x_0 + a$ . The separation distance is  $2x_0 = 2.5a$  and  $K = 0$  (100% depletion).

system is affected by two neighboring bubbles with comparable effects. The field is markedly reduced in the region nearest a neighboring bubble (point B in figure 4).

Figure 4 also shows the distortion in the electric field which renders the system non-steady-state, as in the two-bubble case. The drift velocity (dashed lines) has an east-west (horizontal) component that may be a significant fraction of the vertical velocity. For example,

$|E_y^*/(E_x^* - E_o^*)| \approx 0.48$  at  $\theta = \pi/8$  from the point B just inside the boundary of the central bubble and  $|E_y^*/(E_x^* - E_o^*)| \approx 0.55$  at  $\theta = \pi/8$  from the point  $x = x_o - a$  and  $y = 0$  just inside the boundary of the side bubble. Thus, in the neighborhood of these points, the bubble elements should have significant horizontal drifts.

In addition to the distortion of bubble contours resulting from the non-uniform electric field, the figure also shows that the electric field is substantially reduced from that of an isolated single bubble. This fact is illustrated in figure 5 which gives  $R_3 \equiv |V_y/V_1|$  for the points A, B and C corresponding to  $x = 0$ ,  $x = a$  and  $x = 2x_o + a$ , all just inside the bubble surfaces. Here,  $V_y$  is the vertical drift velocity of the three-bubble system relative to the distant ionosphere. Comparing figure 5 with figure 3, we note that the qualitative behaviour of the rise velocity is similar in both systems, exhibiting significant reduction from that of a single bubble system. However, in the three bubble configuration, the electric field inside the central bubble is substantially weaker than the two neighboring bubbles. Thus, the central bubble has the slowest rise velocity. The line D in figure 5 gives the relative vertical rise velocity of a five-bubble system calculated at  $x = a$ . Curve D, to be compared with curve B, shows that the influence of the additional bubble on the field inside the central bubble is small. The reduction in rise velocities is increased as the number of bubbles is increased. However, the influence of the bubbles beyond the third nearest neighbor is small. In figure 6, we show the relative vertical velocity  $R = V_y/V_1$  as a function of  $N$ , the number of bubbles, for several values of  $x_o$ . For a given separation distance, the rise velocity decreases with increasing  $N$  and levels off for  $N > 3$ . Thus, a three-bubble system describes well the basic morphology of an  $N$ -bubble system.

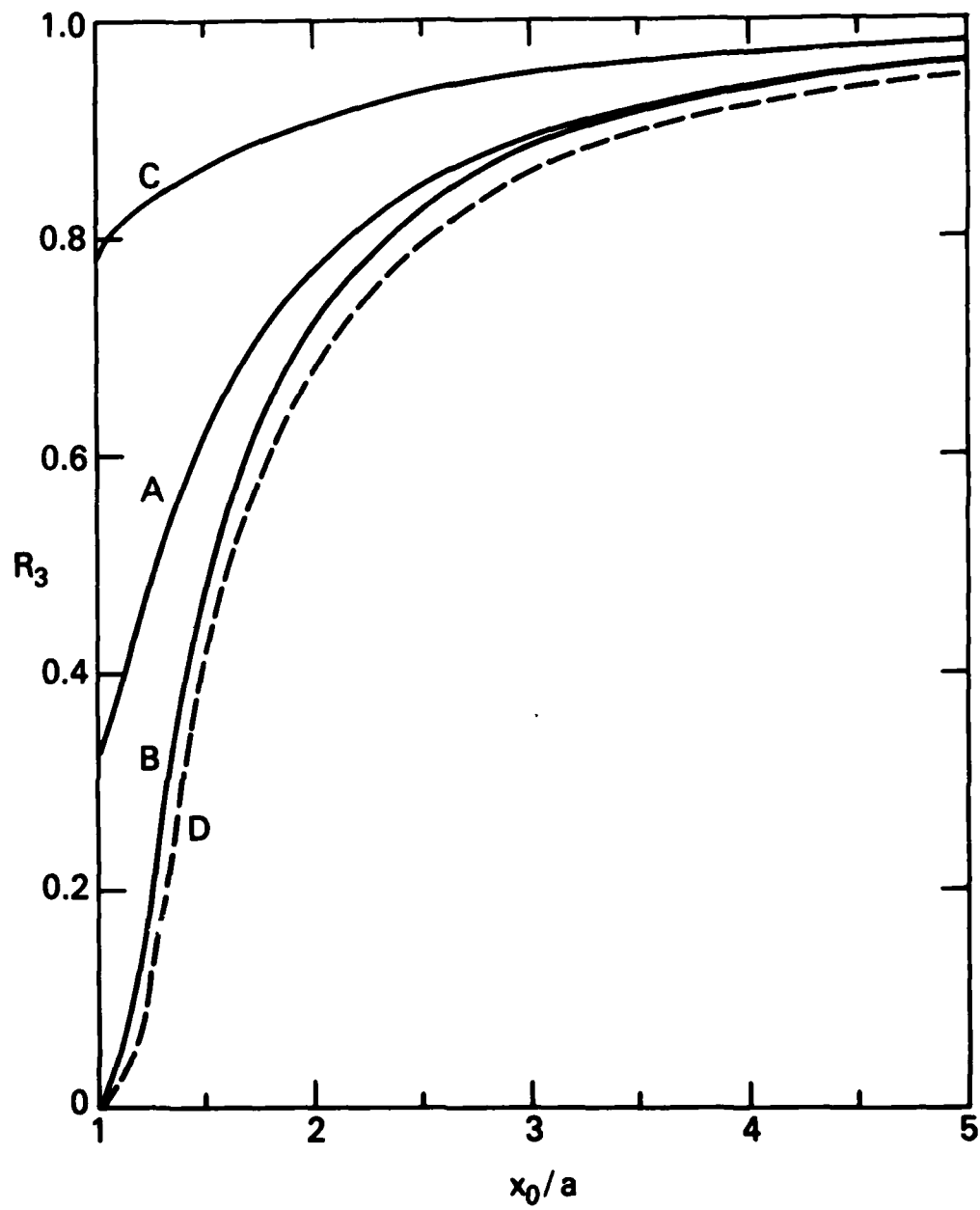


Fig. 5 The ratio  $R_3$  of the vertical velocity  $V_y$  of a three-bubble system to the single-bubble rise velocity  $V_1$ , plotted versus  $x_0/a$ . The curves A, B, and C correspond to the points A, B, and C in figure 4. The curve D (dashed) corresponds to  $R_5 = V_y/V_1$  at  $x = a$  in a five-bubble system, to be compared with the curve B.

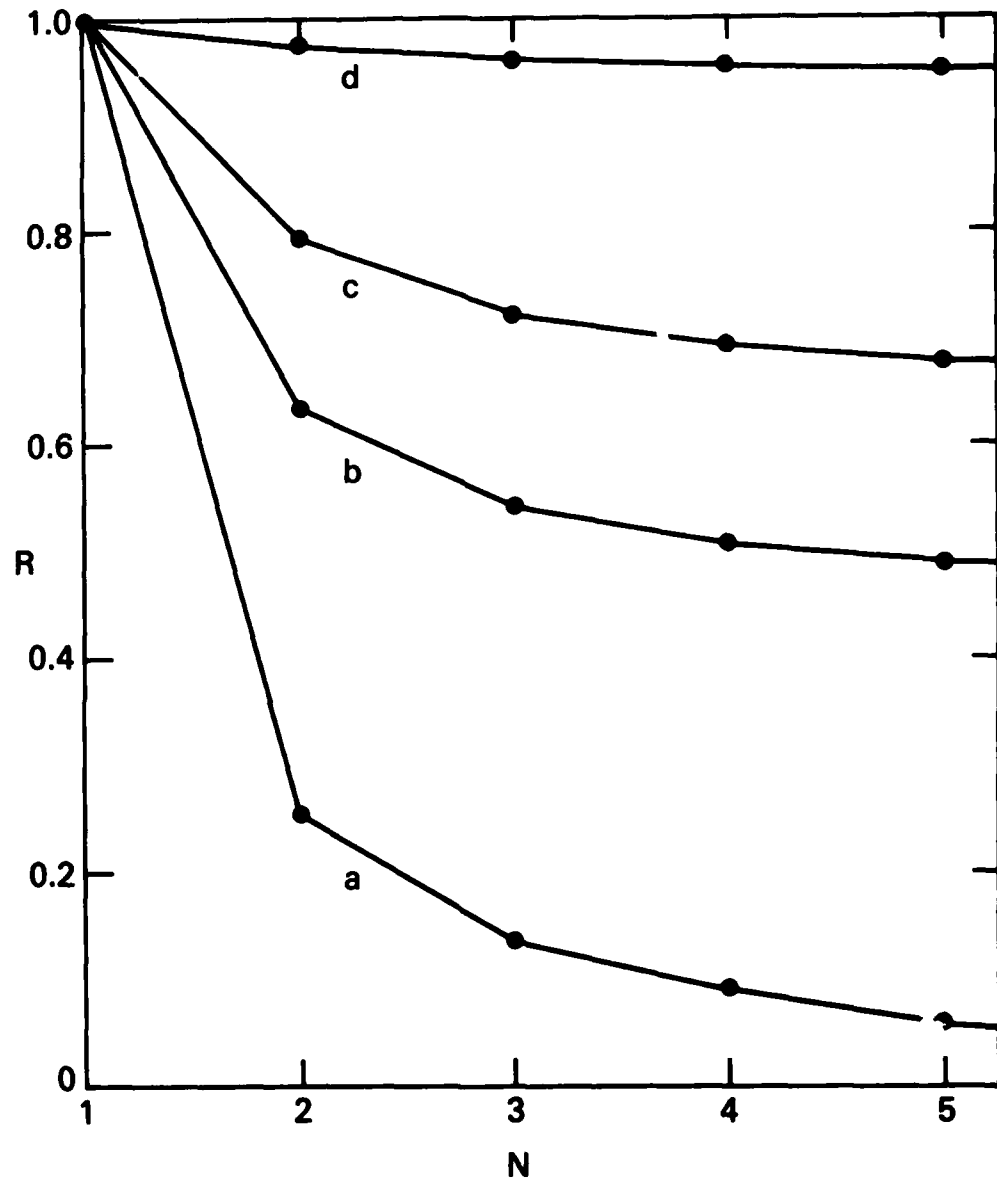


Fig. 6  $R = v_y/v_1$  versus  $N$ , the number of bubbles, evaluated inside at  $x = x_0 - a$  for the two-bubble case and at  $x = a$  for all others.  $K = 0$ . The separation distances ( $2x_0$ ) are (a)  $2x_0 = 2.5a$ , (b)  $2x_0 = 3.2a$ , (c)  $2x_0 = 4.0a$ , and (d)  $2x_0 = 10a$ .

Figures 3 and 5 show that the vertical drift velocity of a bubble is a sensitive function of the separation distance ( $2x_0$ ) except for relatively large values ( $2x_0/a \gtrsim 6$ ). In the context of the Rayleigh-Taylor instability, this implies that the electric field configuration and the drift velocities may depend sensitively on wavelengths ( $2x_0$ ).

As a general remark, we point out that the preceding results derived for plasma density depletions for which  $K < 1$  are also applicable to plasma density enhancements (clouds) for which  $K > 1$ . Calculations for the cloud case show that the electric field configurations are qualitatively similar to that of the bubble case (figures 2 and 4). In particular, the electric field inside the clouds experiences the greatest reduction in the regions facing the neighboring clouds. However, the boundary condition  $K(E_{in})_1 = (E_{out})_1$  implies that  $(E_{in})_1$  is smaller than  $(E_{out})_1$  by a factor of  $K^{-1}$  for clouds. Thus, for a given separation distance  $2x_0$ , the relative distortion in the electric field lines inside a cloud is less pronounced than in a bubble.

Finally, in figure 7, we have plotted the vertical drift velocity versus  $K \equiv n_1/n_2$  for a two-bubble ( $K < 1$ ) and two-cloud ( $K > 1$ ) system. The velocity is calculated at  $x = \pm (x_0 - a)$  (point A in figure 2) and is upward for bubbles and downward for clouds. The velocity is normalized to  $V_1$  (equation (27)) for each value of  $K$ . Note that the point with  $K = 1$  does not exist for each line. For  $K = 1$ , the ionosphere is not disturbed and there is no bubble or cloud drifting vertically. This is born out by the fact that the drift velocity vanishes for a single-bubble (cloud) and any multi-bubble (cloud) system. Clearly, the velocities vanish differently for different separation distances. Mathematically, the ratio of the vertical drift velocity  $V_y = c(E_x^* - E_0)/B_0$  to the single-bubble (cloud) drift velocity  $V_1$  has the limit

$$\frac{V_y}{V_1} = - \left[ 1 - \frac{2}{1+K} a^2 f(x + x_0, y) \right]$$

as  $K \rightarrow 1$ . The circled points in figure 7 correspond to the absolute value of the quantity which has no physical meaning.

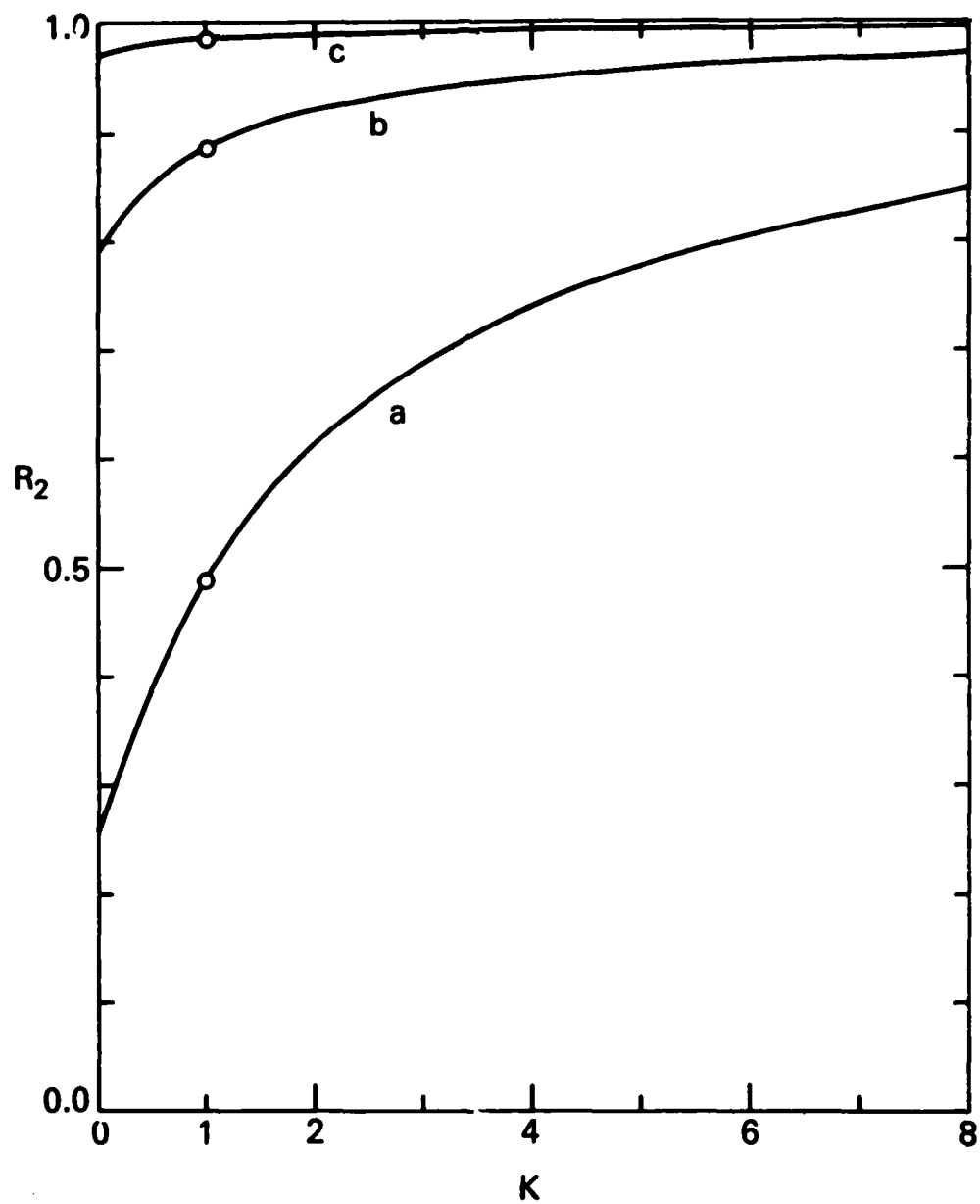


Fig. 7  $R_2 = v_y/v_1$  versus.  $K$  for two-bubble ( $K < 1$ ) and two-cloud ( $K > 1$ ) systems. The separation distances ( $2x_0$ ) are (a)  $2x_0 = 2.5a$ , (b)  $2x_0 = 4a$ , and (c)  $2x_0 = 10a$ .

#### IV. SUMMARY AND DISCUSSION

In the preceding sections, we have solved the current conservation equation (1) with quasi-neutrality for two-bubble and three-bubble systems using a dielectric analogy. These two configurations include the dominant near-neighbor interaction and can model the essential morphology of the multi-bubble systems described. This is demonstrated by actually calculating the field including up to five bubbles. The solutions are exact, satisfying the specified boundary conditions on all the multiple disconnected boundary surfaces and at infinity.

Equations (19), (20), (24) and (25) give the solution of the two-bubble system as a superposition of image line dipole moments. Similar expressions are obtained for three- and N-bubble (cloud) systems ( $N > 3$ ). In all cases, the interaction is dominated by the nearest neighbors and is sensitive to the separation distance ( $2x_0$ ) between bubbles. An important result is that the electric field inside the bubbles is generally highly non-uniform so that the multi-bubble and multi-cloud systems are not steady-state configurations even with piecewise constant density profiles (figures 2 and 4). Moreover, the electric field inside the bubbles is significantly weaker than that in a one-bubble system so that the vertical drift velocity relative to the undisturbed ionosphere is slower than the one-bubble case (equation (27) and figures 3 and 5). For moderately small center-to-center separation distances,  $2x_0 \lesssim 6a$ , the reduction in the rise velocity is substantial. This implies that the electric field configuration and the  $\underline{E} \times \underline{B}$  drift velocity may depend sensitively on the wavelengths of instabilities causing the initial density fluctuations (e.g., the Rayleigh-Taylor instability). In particular, the bubbles with smaller wavelength-to-radius ratio would rise more slowly and be distorted more strongly. This conclusion may be particularly applicable to the initial linear or early-time non-linear stages of the evolution. It has also been shown that in some regions inside bubbles, the horizontal drift velocity may be comparable to the vertical drift velocity with  $|\underline{E}_y^*/(\underline{E}_x^* - \underline{E}_0)|$  as large as 1/2 (Sections II and III).

A corollary that follows from the non-uniform electric field in the bubbles is that the polarization induced  $\underline{E} \times \underline{B}$  drift velocity is sheared

and that a component of the electric field parallel to the local density gradient is developed in the leading edges of the bubbles. For the simple piecewise constant density profiles used for our analysis, the density gradient is not well defined. In a more realistic density profile, however, some previous model calculations indicate that the electric field component parallel to the density gradient has stabilizing influences on the Rayleigh-Taylor instability [Guzdar et al., 1982] and the  $E \times B$  drift instability [Perkins and Doles, 1975; Huba et al., 1982]. More specifically, these calculations show that velocity shear preferentially stabilizes the short wavelength modes. In light of these results, we suggest that the bifurcation behavior of bubbles and clouds may be inhibited by the presence of nearby bubbles (clouds).

The emphasis of our analysis has primarily been on plasma density depletions (bubbles). However, plasma density enhancements (clouds and striation fingers) can also be treated in a similar fashion [Scannapieco and Ossakow, 1976; Scannapieco et al., 1976; Ossakow and Chaturvedi, 1978]. If a cloud exists in the equatorial or low latitude region, the preceding results are all applicable with the replacement of  $K > 1$  ( $K < 1$  for bubbles) where  $K = n_1/n_2$ . In particular, as the backside of an initial cloud begins to bifurcate, the small  $x_0/a$  and small  $N$  results may be applicable. One point to note is that the electric field inside a two- and three-cloud system with a piecewise constant density profile is similar to that shown in figure 2 and 4 with weaker field strength in the regions facing the neighboring clouds. However, the boundary condition  $K(E_{in})_{\perp} = (E_{out})_{\perp}$  implies that  $(E_{in})_{\perp}$  is smaller than  $(E_{out})_{\perp}$  by a factor of  $K^{-1}$  for clouds. As a result, the distortion in the electric field lines inside a cloud is less pronounced than in a bubble.

#### ACKNOWLEDGEMENTS

We would like to thank Drs. P. Chaturvedi, E. Overman, N. Zabusky, and S. Zalesak for useful discussions. This work has been supported by DNA and ONR.

## REFERENCES

Anderson, D.N., and G. Haerendel, The motion of depleted plasma regions in the equatorial ionosphere, J. Geophys. Res., 84, 1251, 1979.

Balsley, B.B., G. Haerendel, and R.A. Greenwald, Equatorial spread F, recent observations and a new interpretation, J. Geophys. Res., 77, 5625, 1972.

Chaturvedi, P.K., and P. Kaw, Steady state finite amplitude Rayleigh-Taylor modes in Spread F, Geophys. Res. Lett., 2, 381, 1975a.

Chaturvedi, P.K., and P. Kaw, Correction, Geophys. Res. Lett., 2, 499, 1975b.

Dungey, J.W., Convective diffusion in the equatorial F region, J. Atmos. Terr. Phys., 9, 304, 1956.

Fejer, B.G. and M.C. Kelley, Ionospheric irregularities, Rev. Geophys. Space Phys., 18, 401, 1980.

Guzdar, P.N., P. Satyanarayana, J.D. Huba and S.L. Ossakow, Influence of velocity shear on Rayleigh-Taylor instability, Geophys. Res. Lett., 9, 547, 1982.

Haerendel, G., Theory of equatorial spread F, preprint, Max-Planck Inst. fur Astrophys., Munich, 1973.

Hanson, W.B., and J. Santani, Large  $N_i$  gradients below the equatorial F peak, J. Geophys. Res., 78, 1167, 1973.

Huba, J.D., S.L. Ossakow, P. Satyanarayana, and P.N. Guzdar, Linear theory of the  $E \times B$  instability with an inhomogeneous electric field, J. Geophys. Res. (accepted for publication 1982).

Hudson, M.K., and C.F. Kennel, Linear theory of equatorial spread-F, J. Geophys. Res., 80, 4581, 1975.

Hudson, M.K., Spread F bubbles: Nonlinear Rayleigh-Taylor mode in two dimensions, J. Geophys. Res., 83, 3189, 1978.

Kelley, M.C., G. Haerendel, H. Kappler, A. Valenzuela, B.B. Balsley, D.A. Carter, W.L. Ecklund, C.W. Carlson, B. Hausler, and R. Torbert, Evidence for a Rayleigh-Taylor type instability and upwelling of depleted density regions during equatorial spread F, Geophys. Res. Lett., 3, 448, 1976.

Kelley, M.C., and J.P. McClure, Equatorial spread F: A review of recent experimental results, J. Atm. Terr. Phys., 43, 427, 1981.

Linson, L.M., and J.B. Workman, Formation of striations in ionospheric clouds, J. Geophys. Res., 75, 3211, 1970.

Longmire, C.L., On the motion of artificial ion clouds, Los Alamos Nuclear Corp. Report, LANC-N-11, 1970.

McClure, J.P., W.B. Hanson, and J.F. Hoffman, Plasma bubbles and irregularities in the equatorial ionosphere, J. Geophys. Res., 82, 2650, 1977.

Ossakow, S.L., and P.K. Chaturvedi, Morphological studies of rising equatorial spread F bubbles, J. Geophys. Res., 83, 2085, 1978.

Ossakow, S.L., Ionospheric irregularities, Rev. Geophys. Space Phys., 17, 521, 1979.

Ossakow, S.L., S.T. Zalesak, B.E. McDonald, and P.K. Chaturvedi, nonlinear equatorial spread F: Dependence on altitude of the F peak and bottomside background electron density gradient scale length, J. Geophys. Res., 84, 17, 1979.

Ossakow, S.L., Spread F theories - a review, J. Atmos. Terr. Phys., 43, 437, 1981.

Ossakow, S.L., M.J. Keskinen, and S.T. Zalesak, Ionospheric irregularity physics modelling, AIAA-82-0147, January 1982.

Ott, E., Theory of Rayleigh-Taylor bubbles in the equatorial ionosphere, J. Geophys. Res., 83, 2006, 1978.

Overman, E., N.J. Zabusky, and S.L. Ossakow, Ionospheric plasma cloud dynamics via regularized contour dynamics: I. Stability and nonlinear evolution of one contour models, Phys. Fluids (accepted for publication) 1982.

Perkins, F.W., N.J. Zabusky, and J.H. Doles III, Deformation and striation of plasma clouds in the ionosphere, I., J. Geophys. Res., 78, 697, 1973.

Perkins, F.W., and J.H. Doles III, Velocity shear and the E  $\times$  B instability, J. Geophys. Res., 80, 211, 1975.

Scannapieco, A.J., and S.L. Ossakow, Nonlinear equatorial spread F, Geophys. Res. Lett., 3, 451, 1976.

Scannapieco, A.J., S.L. Ossakow, S.R. Goldman, and J.M. Pierre, Plasma cloud late time striation spectra, J. Geophys. Res., 81, 6037, 1976.

Smythe, W.R., Static and Dynamic Electricity, Third edition, p. 95, McGraw-Hill Book Company, New York, 1968.

Szuszczewicz, E.P., R.T. Tsunoda, R. Narcisi, and J.C. Holmes, Coincident radar and rocket observations of equatorial spread F, Geophys. Res. Lett., 7, 537, 1980.

Szuszczewicz, E.P., R.T. Tsunoda, R. Narcisi, and J.C. Holmes, PLUMEX II: A second set of coincident radar and rocket observations of equatorial spread F, Geophys. Res. Lett., 8, 803, 1981.

Volk, H.J., and G. Haerendel, Striation in ionospheric clouds, J. Geophys. Res., 76, 454, 1971.

Woodman, R.F. and C. LaHoz, Radar observations of equatorial irregularities, J. Geophys. Res., 81, 5447, 1976.

Zalesak, S.T., and S.L. Ossakow, Nonlinear equatorial spread F: Spatially large bubbles resulting from large horizontal scale initial perturbations, J. Geophys. Res., 85, 2131, 1980.

Zalesak, S.T., S.L. Ossakow, and P.K. Chaturvedi, Nonlinear equatorial spread F: The effect of neutral winds and background Pedersen conductivity, J. Geophys. Res., 87, 151, 1982.

## DISTRIBUTION LIST

### DEPARTMENT OF DEFENSE

ASSISTANT SECRETARY OF DEFENSE  
COMM, CMD, CONT 7 INTELL  
WASHINGTON, D.C. 20301  
01CY ATTN J. BABCOCK  
01CY ATTN M. EPSTEIN

DIRECTOR  
COMMAND CONTROL TECHNICAL CENTER  
PENTAGON RM B6 685  
WASHINGTON, D.C. 20301  
01CY ATTN C-650  
01CY ATTN C-312 R. MASON

DIRECTOR  
DEFENSE ADVANCED RSCH PROJ AGENCY  
ARCHITECT BUILDING  
1400 WILSON BLVD.  
ARLINGTON, VA. 22209  
01CY ATTN NUCLEAR MONITORING RESEARCH  
01CY ATTN STRATEGIC TECH OFFICE

DEFENSE COMMUNICATION ENGINEER CENTER  
1860 WIEHLE AVENUE  
RESTON, VA. 22090  
01CY ATTN CODE R410  
01CY ATTN CODE R812

DIRECTOR  
DEFENSE COMMUNICATIONS AGENCY  
WASHINGTON, D.C. 20305  
(ADR CNWDI: ATTN CODE 240 FOR)  
01CY ATTN CODE 101B

DEFENSE TECHNICAL INFORMATION CENTER  
CAMERON STATION  
ALEXANDRIA, VA 22314  
02CY

DIRECTOR  
DEFENSE NUCLEAR AGENCY  
WASHINGTON, D.C. 20305  
01CY ATTN STVL  
04CY ATTN TITL  
01CY ATTN DDST  
03CY ATTN RAAE

COMMANDER  
FIELD COMMAND  
DEFENSE NUCLEAR AGENCY  
KIRTLAND, AFB, NM 87115  
01CY ATTN FCPR

DIRECTOR  
INTERSERVICE NUCLEAR WEAPONS SCHOOL  
KIRTLAND AFB, NM 87115  
01CY ATTN DOCUMENT CONTROL

JOINT CHIEFS OF STAFF  
WASHINGTON, D.C. 20301  
01CY ATTN J-3 WWMCCS EVALUATION OFFICE

DIRECTOR  
JOINT STRAT TGT PLANNING STAFF  
OFFUTT AFB  
OMAHA, NE 68113  
01CY ATTN JLTH-2  
01CY ATTN JPST G. GOETZ

CHIEF  
LIVERMORE DIVISION FLD COMMAND DNA  
DEPARTMENT OF DEFENSE  
LAWRENCE LIVERMORE LABORATORY  
P.O. BOX 808  
LIVERMORE, CA 94550  
01CY ATTN FCPR

COMMANDANT  
NATO SCHOOL (SHAPE)  
APO NEW YORK 09172  
01CY ATTN U.S. DOCUMENTS OFFICER

UNDER SECY OF DEF FOR RSCH & ENGRG  
DEPARTMENT OF DEFENSE  
WASHINGTON, D.C. 20301  
01CY ATTN STRATEGIC & SPACE SYSTEMS (OS)

WWMCCS SYSTEM ENGINEERING ORG  
WASHINGTON, D.C. 20305  
01CY ATTN R. CRAWFORD

COMMANDER/DIRECTOR  
ATMOSPHERIC SCIENCES LABORATORY  
U.S. ARMY ELECTRONICS COMMAND  
WHITE SANDS MISSILE RANGE, NM 88002  
01CY ATTN DELAS-EO F. NILES

DIRECTOR  
BMD ADVANCED TECH CTR  
HUNTSVILLE OFFICE  
P.O. BOX 1500  
HUNTSVILLE, AL 35807  
01CY ATTN ATC-T MELVIN T. CAPP  
01CY ATTN ATC-O W. DAVIES  
01CY ATTN ATC-R DON RUSS

PROGRAM MANAGER  
BMD PROGRAM OFFICE  
5001 EISENHOWER AVENUE  
ALEXANDRIA, VA 22333  
01CY ATTN DACS-BMT J. SHEA

CHIEF C-E- SERVICES DIVISION  
U.S. ARMY COMMUNICATIONS CMD  
PENTAGON RM 1B269  
WASHINGTON, D.C. 20310  
01CY ATTN C- E-SERVICES DIVISION

COMMANDER  
FRACOM TECHNICAL SUPPORT ACTIVITY  
DEPARTMENT OF THE ARMY  
FORT MONMOUTH, N.J. 07703  
01CY ATTN DRSEL-NL-RD H. BENNET  
01CY ATTN DRSEL-PL-ENV H. BOMKE  
01CY ATTN J.E. QUIGLEY

COMMANDER  
HARRY DIAMOND LABORATORIES  
DEPARTMENT OF THE ARMY  
2800 POWDER MILL ROAD  
ADELPHI, MD 20783  
(CNWDI-INNER ENVELOPE: ATTN: DELHD-RBH)  
01CY ATTN DELHD-TI M. WEINER  
01CY ATTN DELHD-RB R. WILLIAMS  
01CY ATTN DELHD-NP F. WIMENITZ  
01CY ATTN DELHD-NP C. MOAZED

COMMANDER  
U.S. ARMY COMM-ELEC ENGRG INSTAL AGY  
FT. HUACHUCA, AZ 85613  
01CY ATTN CCC-EMEO GEORGE LANE

COMMANDER  
U.S. ARMY FOREIGN SCIENCE & TECH CTR  
220 7TH STREET, NE  
CHARLOTTESVILLE, VA 22901  
01CY ATTN DRXST-SD  
01CY ATTN R. JONES

COMMANDER  
U.S. ARMY MATERIAL DEV & READINESS CMD  
5001 EISENHOWER AVENUE  
ALEXANDRIA, VA 22333  
01CY ATTN DRCLDC J.A. BENDER

COMMANDER  
U.S. ARMY NUCLEAR AND CHEMICAL AGENCY  
7500 BACKLICK ROAD  
BLDG 2073  
SPRINGFIELD, VA 22150  
01CY ATTN LIBRARY

DIRECTOR  
U.S. ARMY BALLISTIC RESEARCH LABORATORY  
ABERDEEN PROVING GROUND, MD 21005  
01CY ATTN TECH LIBRARY EDWARD BAICY

COMMANDER  
U.S. ARMY SATCOM AGENCY  
FT. MONMOUTH, NJ 07703  
01CY ATTN DOCUMENT CONTROL

COMMANDER  
U.S. ARMY MISSILE INTELLIGENCE AGENCY  
REDSTONE ARSENAL, AL 35809  
01CY ATTN JIM GAMBLE

DIRECTOR  
U.S. ARMY TRADOC SYSTEMS ANALYSIS ACTIVITI  
WHITE SANDS MISSILE RANGE, NM 88002  
01CY ATTN ATAA-SA  
01CY ATTN TCC/F. PAYAN JR.  
01CY ATTN ATTA-TAC LTC J. HESSE

COMMANDER  
NAVAL ELECTRONIC SYSTEMS COMMAND  
WASHINGTON, D.C. 20360  
01CY ATTN NAVALEX 034 T. HUGHES  
01CY ATTN PME 117  
01CY ATTN PME 117-T  
01CY ATTN CODE 5011

COMMANDING OFFICER  
NAVAL INTELLIGENCE SUPPORT CTR  
4301 SUITLAND ROAD, BLDG. 5  
WASHINGTON, D.C. 20390  
01CY ATTN MR. DUBBIN STIC 12  
01CY ATTN NISC-50  
01CY ATTN CODE 5404 J. GALET

COMMANDER  
NAVAL OCCEAN SYSTEMS CENTER  
SAN DIEGO, CA 92152  
03CY ATTN CODE 532 W. MOLER  
01CY ATTN CODE 0230 C. BAGGETT  
01CY ATTN CODE 81 R. EASTMAN

DIRECTOR

NAVAL RESEARCH LABORATORY  
WASHINGTON, D.C. 20375

01CY ATTN CODE 4700 S. L. Ossakow  
26 CYS IF UNCLASS. 1 CY IF CLASS)  
01CY ATTN CODE 4701 JACK D. BROWN  
01CY ATTN CODE 4780 BRANCH HEAD (100  
CYS IF UNCLASS, 1 CY IF CLASS)  
01CY ATTN CODE 7500  
01CY ATTN CODE 7550  
01CY ATTN CODE 7580  
01CY ATTN CODE 7551  
01CY ATTN CODE 7555  
01CY ATTN CODE 4730 E. MCLEAN  
01CY ATTN CODE 4187  
20CY ATTN CODE 2628

COMMANDER

NAVAL SEA SYSTEMS COMMAND  
WASHINGTON, D.C. 20362  
01CY ATTN CAPT R. PITKIN

COMMANDER

NAVAL SPACE SURVEILLANCE SYSTEM  
DAHlgren, VA 22448  
01CY ATTN CAPT J.H. BURTON

OFFICER-IN-CHARGE

NAVAL SURFACE WEAPONS CENTER  
WHITE OAK, SILVER SPRING, MD 20910  
01CY ATTN CODE F31

DIRECTOR

STRATEGIC SYSTEMS PROJECT OFFICE  
DEPARTMENT OF THE NAVY  
WASHINGTON, D.C. 20376  
01CY ATTN NSP-2141  
01CY ATTN NSSP-2722 FRED WIMBERLY

COMMANDER

NAVAL SURFACE WEAPONS CENTER  
DAHlgren LABORATORY  
DAHlgren, VA 22448  
01CY ATTN CODE DF-14 R. BUTLER

OFFICER OF NAVAL RESEARCH

ARLINGTON, VA 22217  
01CY ATTN CODE 465  
01CY ATTN CODE 461  
01CY ATTN CODE 402  
01CY ATTN CODE 420  
01CY ATTN CODE 421

COMMANDER

AEROSPACE DEFENSE COMMAND/DC  
DEPARTMENT OF THE AIR FORCE  
ENT AFB, CO 80912  
01CY ATTN DC MR. LONG

COMMANDER

AEROSPACE DEFENSE COMMAND/XPD

DEPARTMENT OF THE AIR FORCE

ENT AFB, CO 80912

01CY ATTN XPDQQ

01CY ATTN XP

AIR FORCE GEOPHYSICS LABORATORY

HANSOM AFB, MA 01731

01CY ATTN OPR HAROLD GARDNER

01CY ATTN LKB KENNETH S.W. CHAMPION

01CY ATTN OPR ALVA T. STAIR

01CY ATTN PHP JULES AARONS

01CY ATTN PHD JURGEN BUCHAU

01CY ATTN PHD JOHN P. MULLEN

AF WEAPONS LABORATORY

KIRTLAND AFT, NM 87117

01CY ATTN SUL

01CY ATTN CA ARTHUR H. GUENTHER

01CY ATTN NTYCE 1LT. G. KRAJEI

AFTAC

PATRICK AFB, FL 32925

01CY ATTN TF/MAJ WILEY

01CY ATTN TN

AIR FORCE AVIONICS LABORATORY

WRIGHT-PATTERSON AFB, OH 45433

01CY ATTN AAD WADE HUNT

01CY ATTN AAD ALLEN JOHNSON

DEPUTY CHIEF OF STAFF

RESEARCH, DEVELOPMENT, & ACQ

DEPARTMENT OF THE AIR FORCE

WASHINGTON, D.C. 20330

01CY ATTN AFRDQ

HEADQUARTERS

ELECTRONIC SYSTEMS DIVISION/XR

DEPARTMENT OF THE AIR FORCE

HANSOM AFB, MA 01731

01CY ATTN XR J. DEAS

HEADQUARTERS

ELECTRONIC SYSTEMS DIVISION/YSEA

DEPARTMENT OF THE AIR FORCE

HANSOM AFB, MA 01732

01CY ATTN YSEA

HEADQUARTERS

ELECTRONIC SYSTEMS DIVISION/DC

DEPARTMENT OF THE AIR FORCE

HANSOM AFB, MA 01731

01CY ATTN DCKC MAJ J.C. CLARK

**COMMANDER**  
 FOREIGN TECHNOLOGY DIVISION, AFSC  
 WRIGHT-PATTERSON AFB, OH 45433  
 O1CY ATTN NICD LIBRARY  
 O1CY ATTN ETDP B. BALLARD

**COMMANDER**  
 ROME AIR DEVELOPMENT CENTER, AFSC  
 GRIFFISS AFB, NY 13441  
 O1CY ATTN DOC LIBRARY/TSLD  
 O1CY ATTN OCSE V. COYNE

**SAMSO/SZ**  
 POST OFFICE BOX 92960  
 WORLDWAY POSTAL CENTER  
 LOS ANGELES, CA 90009  
 (SPACE DEFENSE SYSTEMS)  
 O1CY ATTN SZJ

**STRATEGIC AIR COMMAND/XPFS**  
 OFFUTT AFB, NB 68113  
 O1CY ATTN XPFS MAJ B. STEPHAN  
 O1CY ATTN ADWATE MAJ BRUCE BAUER  
 O1CY ATTN NRI  
 O1CY ATTN DOK CHIEF SCIENTIST

**SAMSO/SK**  
 P.O. BOX 92960  
 WORLDWAY POSTAL CENTER  
 LOS ANGELES, CA 90009  
 O1CY ATTN SKA (SPACE COMM SYSTEMS)  
 M. CLAVIN

**SAMSO/MN**  
 NORTON AFB, CA 92409  
 (MINUTEMAN)  
 O1CY ATTN MNML LTC KENNEDY

**COMMANDER**  
 ROME AIR DEVELOPMENT CENTER, AFSC  
 HANSCOM AFB, MA 01731  
 O1CY ATTN EEP A. LORENTZEN

**DEPARTMENT OF ENERGY**  
 LIBRARY ROOM G-042  
 WASHINGTON, D.C. 20545  
 O1CY ATTN DOC CON FOR A. LABOWITZ

**DEPARTMENT OF ENERGY**  
 ALBUQUERQUE OPERATIONS OFFICE  
 P.O. BOX 5400  
 ALBUQUERQUE, NM 87115  
 O1CY ATTN DOC CON FOR D. SHERWOOD

**EG&G, INC.**  
 LOS ALAMOS DIVISION  
 P.O. BOX 809  
 LOS ALAMOS, NM 85544  
 O1CY ATTN DOC CON FOR J. BREEDLOVE

**UNIVERSITY OF CALIFORNIA**  
 LAWRENCE LIVERMORE LABORATORY  
 P.O. BOX 808  
 LIVERMORE, CA 94550  
 O1CY ATTN DOC CON FOR TECH INFO DEP  
 O1CY ATTN DOC CON FOR L-389 R. OTT  
 O1CY ATTN DOC CON FOR L-31 R. HAGER  
 O1CY ATTN DOC CON FOR L-46 F. SEWAR

**LOS ALAMOS NATIONAL LABORATORY**  
 P.O. BOX 1663  
 LOS ALAMOS, NM 87545  
 O1CY ATTN DOC CON FOR J. WOLCOTT  
 O1CY ATTN DOC CON FOR R.F. TASCHER  
 O1CY ATTN DOC CON FOR E. JONES  
 O1CY ATTN DOC CON FOR J. MALIK  
 O1CY ATTN DOC CON FOR R. JEFFRIES  
 O1CY ATTN DOC CON FOR J. ZINN  
 O1CY ATTN DOC CON FOR P. KEATON  
 O1CY ATTN DOC CON FOR D. WESTERVELT

**SANDIA LABORATORIES**  
 P.O. BOX 5800  
 ALBUQUERQUE, NM 87115  
 O1CY ATTN DOC CON FOR W. BROWN  
 O1CY ATTN DOC CON FOR A. THORNBROUG  
 O1CY ATTN DOC CON FOR T. WRIGHT  
 O1CY ATTN DOC CON FOR D. DAHLGREN  
 O1CY ATTN DOC CON FOR 3141  
 O1CY ATTN DOC CON FOR SPACE PROJECT

**SANDIA LABORATORIES**  
 LIVERMORE LABORATORY  
 P.O. BOX 969  
 LIVERMORE, CA 94550  
 O1CY ATTN DOC CON FOR B. MURPHAY  
 O1CY ATTN DOC CON FOR T. COOK

**OFFICE OF MILITARY APPLICATION**  
**DEPARTMENT OF ENERGY**  
 WASHINGTON, D.C. 20545  
 O1CY ATTN DOC CON DR. YO SONG

**OTHER GOVERNMENT**  
**DEPARTMENT OF COMMERCE**  
**NATIONAL BUREAU OF STANDARDS**  
 WASHINGTON, D.C. 20234  
 (ALL CORRES: ATTN SEC OFFICER FOR)  
 O1CY ATTN R. MOORE

INSTITUTE FOR TELECOM SCIENCES  
NATIONAL TELECOMMUNICATIONS & INFO ADMIN  
BOULDER, CO 80303  
01CY ATTN A. JEAN (UNCLASS ONLY)  
01CY ATTN W. UTLAUT  
01CY ATTN D. CROMBIE  
01CY ATTN L. BERRY

NATIONAL OCEANIC & ATMOSPHERIC ADMIN  
ENVIRONMENTAL RESEARCH LABORATORIES  
DEPARTMENT OF COMMERCE  
BOULDER, CO 80302  
01CY ATTN R. GRUBB  
01CY ATTN AERONOMY LAB G. REID

DEPARTMENT OF DEFENSE CONTRACTORS

AEROSPACE CORPORATION  
P.O. BOX 92957  
LOS ANGELES, CA 90009  
01CY ATTN I. GARFUNKEL  
01CY ATTN T. SALMI  
01CY ATTN V. JOSEPHSON  
01CY ATTN S. BOWER  
01CY ATTN N. STOCKWELL  
01CY ATTN D. OLSEN

ANALYTICAL SYSTEMS ENGINEERING CORP  
5 OLD CONCORD ROAD  
BURLINGTON, MA 01803  
01CY ATTN RADIO SCIENCES

BERKELEY RESEARCH ASSOCIATES, INC.  
P.O. BOX 983  
BERKELEY, CA 94701  
01CY ATTN J. WORKMAN  
01CY ATTN C. PRETTIE

BOEING COMPANY, THE  
P.O. BOX 3707  
SEATTLE, WA 98124  
01CY ATTN G. KEISTER  
01CY ATTN D. MURRAY  
01CY ATTN G. HALL  
01CY ATTN J. KENNEY

BROWN ENGINEERING COMPANY, INC.  
CUMMINGS RESEARCH PARK  
HUNTSVILLE, AL 35807  
01CY ATTN ROMEO A. DELIBERIS

CALIFORNIA AT SAN DIEGO, UNIV OF  
P.O. BOX 6049  
SAN DIEGO, CA 92106

CHARLES STARK DRAPER LABORATORY, INC.  
555 TECHNOLOGY SQUARE  
CAMBRIDGE, MA 02139  
01CY ATTN D.B. COX  
01CY ATTN J.P. GILMORE

COMSAT LABORATORIES  
LINTHICUM ROAD  
CLARKSBURG, MD 20734  
01CY ATTN G. HYDE

CORNELL UNIVERSITY  
DEPARTMENT OF ELECTRICAL ENGINEERING  
ITHACA, NY 14850  
01CY ATTN D.T. FARLEY, JR.

ELECTROSPACE SYSTEMS, INC.  
BOX 1359  
RICHARDSON, TX 75080  
01CY ATTN H. LOGSTON  
01CY ATTN SECURITY (PAUL PHILLIPS)

ESL, INC.  
495 JAVA DRIVE  
SUNNYVALE, CA 94086  
01CY ATTN J. ROBERTS  
01CY ATTN JAMES MARSHALL

GENERAL ELECTRIC COMPANY  
SPACE DIVISION  
VALLEY FORGE SPACE CENTER  
GODDARD BLVD KING OF PRUSSIA  
P.O. BOX 8555  
PHILADELPHIA, PA 19101  
01CY ATTN M.H. BORTNER SPACE SCI LAB

GENERAL ELECTRIC COMPANY  
P.O. BOX 1122  
SYRACUSE, NY 13201  
01CY ATTN F. REIBERT

GENERAL ELECTRIC TECH SERVICES CO., INC  
HMES  
COURT STREET  
SYRACUSE, NY 13201  
01CY ATTN G. MILLMAN

GENERAL RESEARCH CORPORATION  
SANTA BARBARA DIVISION  
P.O. BOX 6770  
SANTA BARBARA, CA 93111  
01CY ATTN JOHN ISE, JR.  
01CY ATTN JOEL GARBARINO

GEOGRAPHICAL INSTITUTE  
UNIVERSITY OF ALASKA  
FAIRBANKS, AK 99701  
(ALL CLASS ATTN: SECURITY OFFICER)  
01CY ATTN T.N. DAVIS (UNCLASS ONLY)  
01CY ATTN TECHNICAL LIBRARY  
01CY ATTN NEAL BROWN (UNCLASS ONLY)

GTE SYLVANIA, INC.  
ELECTRONICS SYSTEMS GRP-EASTERN DIV  
77 A STREET  
NEEDHAM, MA 02194  
01CY ATTN MARSHALL CROSS

HSS, INC.  
2 ALFRED CIRCLE  
BEDFORD, MA 01730  
01CY ATTN DONALD HANSEN

ILLINOIS, UNIVERSITY OF  
107 COBLE HALL  
150 DAVENPORT HOUSE  
CHAMPAIGN, IL 61820  
(ALL CORRES ATTN DAN MCCLELLAND)  
01CY ATTN K. YEH

INSTITUTE FOR DEFENSE ANALYSES  
400 ARMY-NAVY DRIVE  
ARLINGTON, VA 22202  
01CY ATTN J.M. AEIN  
01CY ATTN ERNEST BAUER  
01CY ATTN HANS WOLFARD  
01CY ATTN JOEL BENGSTON

INTL TEL & TELEGRAPH CORPORATION  
500 WASHINGTON AVENUE  
NUTLEY, NJ 07110  
01CY ATTN TECHNICAL LIBRARY

JAYCOR  
11011 TORREYANA ROAD  
P.O. BOX 85154  
SAN DIEGO, CA 92138  
01CY ATTN J.L. SPERLING

JOHNS HOPKINS UNIVERSITY  
APPLIED PHYSICS LABORATORY  
JOHNS HOPKINS ROAD  
LAURAL, MD 20810  
01CY ATTN DOCUMENT LIBRARIAN  
01CY ATTN THOMAS POTEMRA  
01CY ATTN JOHN DASSOULAS

KAMAN SCIENCES CORP  
P.O. BOX 7463  
COLORADO SPRINGS, CO 80933  
01CY ATTN T. MEACHER

KAMAN TEMPO-CENTER FOR ADVANCED STUD:  
816 STATE STREET (P.O DRAWER QQ)  
SANTA BARBARA, CA 93102  
01CY ATTN DASIA  
01CY ATTN TIM STEPHANS  
01CY ATTN WARREN S. KNAPP  
01CY ATTN WILLIAM McNAMARA  
01CY ATTN B. GAMBILL

LINKABIT CORP  
10453 ROSELLE  
SAN DIEGO, CA 92121  
01CY ATTN IRWIN JACOBS

LOCKHEED MISSILES & SPACE CO., INC  
P.O. BOX 504  
SUNNYVALE, CA 94088  
01CY ATTN DEPT 60-12  
01CY ATTN D.R. CHURCHILL

LOCKHEED MISSILES & SPACE CO., INC.  
3251 HANOVER STREET  
PALO ALTO, CA 94304  
01CY ATTN MARTIN WALT DEPT 52-12  
01CY ATTN W.L. IMHOFF DEPT 52-12  
01CY ATTN RICHARD G. JOHNSON DEPT  
01CY ATTN J.B. CLADIS DEPT 52-12

LOCKHEED MISSILE & SPACE CO., INC.  
HUNTSVILLE RESEARCH & ENGR. CTR.  
4800 BRADFORD DRIVE  
HUNTSVILLE, AL 35807  
ATTN DALE H. DIVIS

MARTIN MARIETTA CORP  
ORLANDO DIVISION  
P.O. BOX 5837  
ORLANDO, FL 32805  
01CY ATTN R. HEFFNER

M.I.T. LINCOLN LABORATORY  
P.O. BOX 73  
LEXINGTON, MA 02173  
01CY ATTN DAVID M. TOWLE  
01CY ATTN P. WALDRON  
01CY ATTN L. LOUGHIN  
01CY ATTN D. CLARK

MCDONNELL DOUGLAS CORPORATION  
5301 BOLSA AVENUE  
HUNTINGTON BEACH, CA 92647  
01CY ATTN N. HARRIS  
01CY ATTN J. MOULE  
01CY ATTN GEORGE MROZ  
01CY ATTN W. OLSON  
01CY ATTN R.W. HALPRIN  
01CY ATTN TECHNICAL LIBRARY SERVICE

MISSION RESEARCH CORPORATION  
735 STATE STREET  
SANTA BARBARA, CA 93101  
01CY ATTN P. FISCHER  
01CY ATTN W.F. CREVIER  
01CY ATTN STEVEN L. GUTSCHE  
01CY ATTN D. SAPPENFIELD  
01CY ATTN R. BOGUSCH  
01CY ATTN R. HENDRICK  
01CY ATTN RALPH KILB  
01CY ATTN DAVE SOWLE  
01CY ATTN F. FAJEN  
01CY ATTN M. SCHEIBE  
01CY ATTN CONRAD L. LONGMIRE  
01CY ATTN WARREN A. SCHLUETER

MITRE CORPORATION, THE  
P.O. BOX 208  
BEDFORD, MA 01730  
01CY ATTN JOHN MORGANSTERN  
01CY ATTN G. HARDING  
01CY ATTN C.E. CALLAHAN

MITRE CORP  
WESTGATE RESEARCH PARK  
1820 DOLLY MADISON BLVD  
MCLEAN, VA 22101  
01CY ATTN W. HALL  
01CY ATTN W. FOSTER

PACIFIC-SIERRA RESEARCH CORP.  
1456 CLOVERFIELD BLVD.  
SANTA MONICA, CA 90404  
01CY ATTN E.C. FIELD, JR.

PENNSYLVANIA STATE UNIVERSITY  
IONOSPHERE RESEARCH LAB  
318 ELECTRICAL ENGINEERING EAST  
UNIVERSITY PARK, PA 16802  
(NO CLASS TO THIS ADDRESS)  
01CY ATTN IONOSPHERIC RESEARCH LAB

PHOTOMETRICS, INC.  
442 MARRETT ROAD  
LEXINGTON, MA 02173  
01CY ATTN IRVING L. KOFSKY

PHYSICAL DYNAMICS, INC.  
P.O. BOX 3027  
BELLEVUE, WA 98009  
01CY ATTN E.J. FREMOUW

PHYSICAL DYNAMICS, INC.  
P.O. BOX 10367  
OAKLAND, CA 94610  
ATTN A. THOMSON

R & D ASSOCIATES  
P.O. BOX 9695  
MARINA DEL REY, CA 90291  
01CY ATTN FORREST GILMORE  
01CY ATTN BRYAN GABBARD  
01CY ATTN WILLIAM B. WRIGHT, JR.  
01CY ATTN ROBERT F. LELEVIER  
01CY ATTN WILLIAM J. KARZAS  
01CY ATTN H. ORY  
01CY ATTN C. MACDONALD  
01CY ATTN R. TURCO

RAND CORPORATION, THE  
1700 MAIN STREET  
SANTA MONICA, CA 90406  
01CY ATTN CULLEN CRAIN  
01CY ATTN ED BEDROZIAN

RAYTHEON CO.  
528 BOSTON POST ROAD  
SUDBURY, MA 01776  
01CY ATTN BARBARA ADAMS

RIVERSIDE RESEARCH INSTITUTE  
80 WEST END AVENUE  
NEW YORK, NY 10023  
01CY ATTN VINCE TRAPANI

SCIENCE APPLICATIONS, INC.  
P.O. BOX 2351  
LA JOLLA, CA 92038  
01CY ATTN LEWIS M. LINSON  
01CY ATTN DANIEL A. HAMLIN  
01CY ATTN E. FRIEMAN  
01CY ATTN E.A. STRAKER  
01CY ATTN CURTIS A. SMITH  
01CY ATTN JACK McDougall

SCIENCE APPLICATIONS, INC  
1710 GOODRIDGE DR.  
MCLEAN, VA 22102  
ATTN: J. COCKAYNE

SRI INTERNATIONAL  
333 RAVENSWOOD AVENUE  
MENLO PARK, CA 94025  
O1CY ATTN DONALD NEILSON  
O1CY ATTN ALAN BURNS  
O1CY ATTN G. SMITH  
O1CY ATTN L.L. COBB  
O1CY ATTN DAVID A. JOHNSON  
O1CY ATTN WALTER G. CHESNUT  
O1CY ATTN CHARLES L. RINO  
O1CY ATTN WALTER JAYE  
O1CY ATTN M. BARON  
O1CY ATTN RAY L. LEADABRAND  
O1CY ATTN G. CARPENTER  
O1CY ATTN G. PRICE  
O1CY ATTN J. PETERSON  
O1CY ATTN R. HAKE, JR.  
O1CY ATTN V. GONZALES  
O1CY ATTN D. MCDANIEL

STEWART RADIANCE LABORATORY  
UTAH STATE UNIVERSITY  
1 DE ANGELO DRIVE  
BEDFORD, MA 01730  
O1CY ATTN J. ULWICK

TECHNOLOGY INTERNATIONAL CORP  
75 WIGGINS AVENUE  
BEDFORD, MA 01730  
O1CY ATTN W.P. BOQUIST

TRW DEFENSE & SPACE SYS GROUP  
ONE SPACE PARK  
REDONDO BEACH, CA 90278  
O1CY ATTN R. K. PLEBUCH  
O1CY ATTN S. ALTSCHULER  
O1CY ATTN D. DEE

VISIDYNE  
SOUTH BEDFORD STREET  
BURLINGTON, MASS 01803  
O1CY ATTN W. REIDY  
O1CY ATTN J. CARPENTER  
O1CY ATTN C. HUMPHREY

IONOSPHERIC MODELING DISTRIBUTION LIST  
(UNCLASSIFIED ONLY)

PLEASE DISTRIBUTE ONE COPY TO EACH OF THE FOLLOWING PEOPLE (UNLESS OTHERWISE NOTED)

NAVAL RESEARCH LABORATORY  
WASHINGTON, D.C. 20375  
DR. P. MANGE - CODE 4101  
DR. E. SZUSZCZEWCZ - CODE 4187  
DR. J. GOODMAN - CODE 4180  
DR. P. RODRIGUEZ - CODE 4187

NASA  
Code 961  
GODDARD SPACE FLIGHT CENTER  
GREENBELT, MD 20771  
DR. R.F. BENSON  
DR. K. MAEDA  
Dr. S. Curtis  
Dr. M. Dubin

A.F. GEOPHYSICS LABORATORY  
L.G. HANSCOM FIELD  
BEDFORD, MA 01730  
DR. T. ELKINS  
DR. W. SWIDER  
MRS. R. SAGALYN  
DR. J.M. FORBES  
DR. T.J. KENESHEA  
DR. J. AARONS  
DR. H. CARLSON  
DR. J. JASPERSE

NATIONAL TECHNICAL INFORMATION CENTER  
CAMERON STATION  
ALEXANDRIA, VA 22314  
12CY ATTN TC

CORNELL UNIVERSITY  
ITHACA, NY 14850  
DR. W.E. SWARTZ  
DR. R. SUDAN  
DR. D. FARLEY  
DR. M. KELLEY

COMMANDER  
NAVAL AIR SYSTEMS COMMAND  
DEPARTMENT OF THE NAVY  
WASHINGTON, D.C. 20360  
DR. T. CZUBA

HARVARD UNIVERSITY  
HARVARD SQUARE  
CAMBRIDGE, MA 02138  
DR. M.B. McELROY  
DR. R. LINDZEN

COMMANDER  
NAVAL OCEAN SYSTEMS CENTER  
SAN DIEGO, CA 92152  
MR. R. ROSE - CODE 5321

INSTITUTE FOR DEFENSE ANALYSIS  
400 ARMY/NAVY DRIVE  
ARLINGTON, VA 22202  
DR. E. BAUER

NOAA  
DIRECTOR OF SPACE AND ENVIRONMENTAL  
LABORATORY  
BOULDER, CO 80302  
DR. A. GLENN JEAN  
DR. G.W. ADAMS  
DR. D.N. ANDERSON  
DR. K. DAVIES  
DR. R. F. DONNELLY

MASSACHUSETTS INSTITUTE OF TECHNOLOGY  
PLASMA FUSION CENTER  
LIBRARY, NW16-262  
CAMBRIDGE, MA 02139

OFFICE OF NAVAL RESEARCH  
800 NORTH QUINCY STREET  
ARLINGTON, VA 22217  
DR. G. JOINER

PENNSYLVANIA STATE UNIVERSITY  
UNIVERSITY PARK, PA 16802  
DR. J.S. NISBET  
DR. P.R. ROHRBAUGH  
DR. L.A. CARPENTER  
DR. M. LEE  
DR. R. DIVANY  
DR. P. BENNETT  
DR. F. KLEVANS

PRINCETON UNIVERSITY  
PLASMA PHYSICS LABORATORY  
PRINCETON, NJ 08540  
DR. F. PERKINS

SCIENCE APPLICATIONS, INC.  
1150 PROSPECT PLAZA  
LA JOLLA, CA 92037  
DR. D.A. HAMLIN  
DR. L. LINSON  
DR. E. FRIEMAN

STANFORD UNIVERSITY  
STANFORD, CA 94305  
DR. P.M. BANKS

U.S. ARMY ABERDEEN RESEARCH  
AND DEVELOPMENT CENTER  
BALLISTIC RESEARCH LABORATORY  
ABERDEEN, MD  
DR. J. HEIMERL

UNIVERSITY OF CALIFORNIA,  
BERKELEY  
BERKELEY, CA 94720  
DR. M. HUDSON

UNIVERSITY OF CALIFORNIA  
LOS ALAMOS SCIENTIFIC LABORATORY  
J-10, MS-664  
LOS ALAMOS, NM 87545  
M. PONGRATZ  
D. SIMONS  
G. BARASCH  
L. DUNCAN  
P. BERNHARDT

UNIVERSITY OF CALIFORNIA,  
LOS ANGELES  
405 HILLGARD AVENUE  
LOS ANGELES, CA 90024  
DR. F.V. CORONITI  
DR. C. KENNEL  
DR. A.Y. WONG

UNIVERSITY OF MARYLAND  
COLLEGE PARK, MD 20740  
DR. K. PAPADOPOULOS  
DR. E. OTT

UNIVERSITY OF PITTSBURGH  
PITTSBURGH, PA 15213  
DR. N. ZABUSKY  
DR. M. BIONDI  
DR. E. OVERMAN

UTAH STATE UNIVERSITY  
4TH AND 8TH STREETS  
LOGAN, UTAH 84322  
DR. R. HARRIS  
DR. K. BAKER  
DR. R. SCHUNK

